UNIVERSITY OF CRETE

SCHOOL OF SCIENCE AND ENGINEERING

DEPARTMENT OF MATERIALS SCIENCE AND TECNHOLOGY

Photodegradable Hydrogels for Drug Delivery Applications

Bachelor Thesis of:

Ioanna Chatzaki

Supervisor:

Maria Vamvakaki

Heraklion, October 2021

Acknowledgments

First, I would like to express my sincere gratitude to my supervisor Professor Maria Vamvakaki for giving me the opportunity to carry out this bachelor thesis in her lab. I want to thank her for her guidance and her advice throughout the whole year. I would also like to thank Professor Konstantinos Karatasos for participating in my committee.

Next, my special thanks go to the PhD candidate Maria Psarrou for her support, her patience and her useful advice during my research. By sharing her knowledge with me, she helped me develop a scientific way of thinking and broaden my horizons about the field of polymer chemistry. The completion of this study could not have been possible without her.

I would also like to thank my colleagues at the Materials Chemistry Lab for all their support and help. A huge thank you goes to my friends outside the lab for being there for me when I needed them, supporting me and understanding my ups and downs through this process.

Last but not least, the biggest thank you goes to my parents and my little sister. I would like to thank them for their endless love, their encouragement and their support. Even though we were miles apart, I still felt like they were next to me throughout this experience. I could not thank them enough.

Table of Contents

Abstract 1

Chapter 1: Introduction 2

1.1 Stimuli – responsive polymers 2

1.2 Drug delivery 3

1.2.1 Liposomes 4

1.2.2 Dendrimers 4

1.2.3 Polymer micelles 4

1.2.4 Polymer nanoparticles 5

1.3 Polymer hydrogels 5

1.3.1 Photodegradable hydrogels 8

1.3.2 PEG-based hydrogels 8

1.4 Thioacetals 9

1.5 Aim of this work 11

Chapter 2: Experimental 12

2.1 Materials 12

2.2 Characterization methods 12

2.2.1 Proton Nuclear Magnetic Resonance (^{1}H NMR) spectroscopy 12

2.2.2 Scanning Electron Microscopy (SEM) 12

2.2.3 Ultraviolet-Visible (UV-Vis) spectroscopy 13

2.3 Synthesis of dithiol end-functionalized PEG_{4k} 13

2.4 Synthesis of $PEG_n(SH)_2$ – terephthaldehyde ($PEG_n(SH)_2$-TPA) hydrogels 14

2.5 Swelling studies 15

2.6 Photodegradation studies 15

2.7 Encapsulation of hydrophilic or hydrophobic dyes within the hydrogels 16

2.7.1 In situ $PEG_n(SH)_2$-TPA hydrogel formation with the hydrophobic dye Sudan Red 7b 16

2.7.2 Hydrophilic dye Orange II loading within the $PEG_n(SH)_2$-TPA hydrogels 17

2.8 Release studies from the dye loaded hydrogels.....18

2.8.1 Release of Sudan Red 7b from the hydrogels.....18

2.8.2 Release of Orange II from the hydrogels.....18

Chapter 3: Results and discussion.....20

3.1 Synthesis of the dithiol end-functionalized PEG.....20

3.2 Preparation of $PEG_n(SH)_2$ – terephthaldehyde ($PEG_n(SH)_2$-TPA) hydrogels...22

3.3 $PEG_n(SH)_2$-TPA hydrogel characterization.....24

3.4 Swelling studies.....26

3.5 Photodegradation studies of the $PEG_n(SH)_2$–TPA hydrogels.....27

3.6 Dye release studies.....28

3.6.1 Release of the hydrophobic dye loaded in the $PEG_n(SH)_2$-TPA hydrogels.29

3.6.2 Release of the hydrophilic dye loaded in the $PEG_n(SH)_2$-TPA hydrogels...32

Chapter 4: Conclusions and future studies.....35

Chapter 5: Characterization techniques.....37

5.1 Proton Nuclear Magnetic Resonance (^1H NMR) spectroscopy.....37

5.2 Scanning Electron Microscopy (SEM).....38

5.3 Ultraviolet-Visible (UV-Vis) spectroscopy.....38

References.....40

Abstract

Hydrogels are widely used in a variety of biomedical applications, including drug delivery, matrices for the controlled release of biomolecules and scaffolds for regenerative medicine. The aim of the present thesis, is the development of photodegradable hydrogels composed of linear, poly(ethylene glycol) (PEG) chains with different molecular weights (1000 gr/mol, 1500 gr/mol and 4000 gr/mol), and a small, difunctional aromatic comonomer as the crosslinker. Dithiol end-functionalized PEGs with different molecular weights were synthesized in order to be used as the macromonomer. The resulting products were characterized by proton nuclear magnetic resonance (^{1}H NMR) spectroscopy. Hydrogels were prepared at a 1:1 and 2:1 molar ratio of the two components. The prepared thioacetal-based hydrogels were characterized in terms of their swelling degrees and their ability to encapsulate hydrophilic and hydrophobic dye molecules. Moreover, the release profile of a hydrophilic and a hydrophobic dye from the hydrogel in aqueous environments, with and without irradiation at 254 nm, was studied. The porous structure of the prepared hydrogels was characterized by scanning electron microscopy (SEM) which showed that the hydrogels prepared using the 4000 gr/mol PEG dithiol appeared to be highly porous with larger pores compared to the hydrogels prepared using 1000 gr/mol and 1500 gr/mol PEG dithiol. Finally, in order to verify the photodegradation mechanism of the hydrogels, the properties of the thioacetal-based hydrogels were studied during irradiation with UV light at 254 nm.

Chapter 1: Introduction

1.1 Stimuli – responsive polymers

Polymers are ubiquitous in everyday life, and are even responsible for life itself, e.g., DNA and proteins. For ages, polymers have been used to improve the quality of life [1]. After years of research on the field of polymers, this combined knowledge has allowed the development of polymers for nearly every imaginable application, and is single-handedly responsible for the good quality of life. This foundational research has also led to the development of a new class of polymers, which respond to their environment by changing their physical and/or chemical properties [2]. These polymers, referred to as stimuli-responsive polymers (or "smart" polymers), are synthesized to respond to a variety of stimuli, such as the solution pH [3] and temperature [4], the presence of various small molecules and biomolecules [5], electric/magnetic fields [6] etc. (**Fig. 1.1**) "Smart" polymers have found many applications in the fields of biology and medicine, and can be used as sensors and biosensors [7], chemo-mechanical actuators [8–10], for controlled and triggered drug delivery [11], but also for environmental remediation [12].

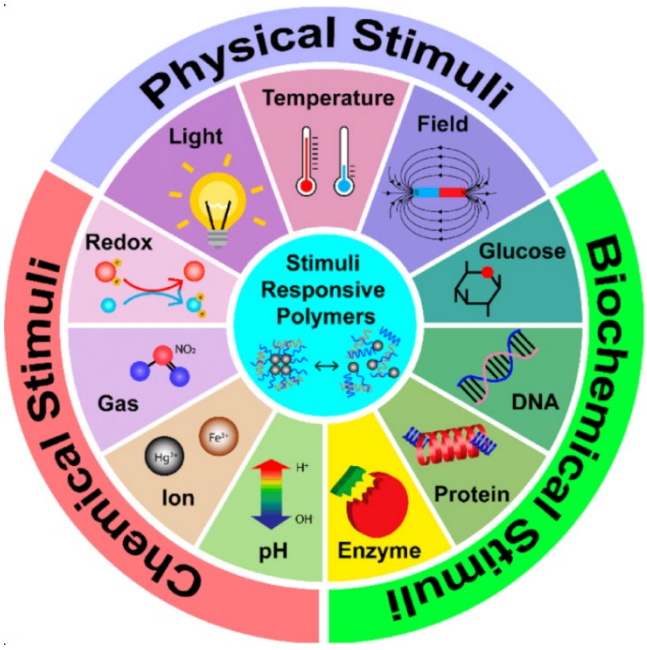

Figure 1.1: Physical, chemical, and biochemical responsiveness of stimuli-responsive polymers [13].

1.2 Drug delivery

Drug delivery is the method of administrating a pharmaceutical compound to achieve a therapeutic effect in humans or animals [14]. Drug delivery systems (DDS) are designed to improve the pharmacological and therapeutic properties of drugs [15]. Polymers have played an integral role in the advancement of the drug delivery technology by providing controlled release of therapeutic agents at constant doses over long periods, cyclic dosage, and tunable release of both hydrophilic and hydrophobic drugs [16].

Multiple types of DDS have been developed using a broad range of organic and inorganic materials (**Fig. 1.2**) including polymeric nanocarriers (nanoparticles, dendrimers), lipidic/surfactant-based nanocarriers (liposomes, micelles), hydrogels (polymeric networks) etc. The selection of a suitable carrier system and material should be done on the basis of the desired diagnostic and/or therapeutic goal, physicochemical properties of the drug substance, material safety profile, and the route of administration [17]. Among them, polymer hydrogels have been used by many investigators in controlled-release drug delivery systems, because of their good tissue compatibility and facile manipulation of their degree of swelling [18].

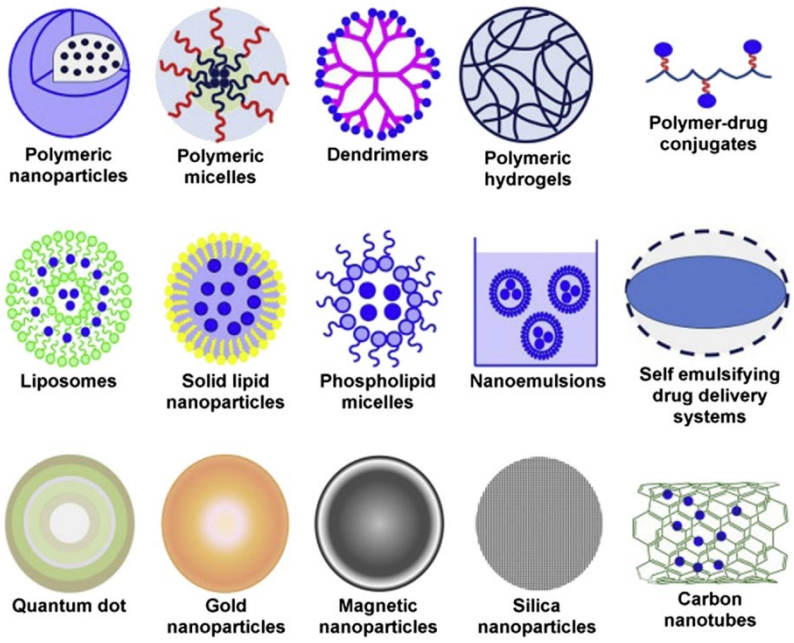

Figure 1.2: Different types of drug delivery systems [17].

1.2.1 Liposomes

Liposomes are bubble-like microscopic bilayered structures made of phospholipids [17]. Since their discovery in the 1960s, liposomes have been studied in depth, and they continue to constitute a field of intense research. Liposomes are valued for their biological and technological advantages, and are considered to be the most successful drug-carrier system known to date. FDA-approved liposome technologies against cancer exist, with Doxil being the first pharmaceutical product in a liposomal formulation that received FDA approval at 1995 [19]. Liposomes can be easily formulated by hydrating phospholipids in an excess aqueous medium. A very impressive characteristic of liposomes is that they can encapsulate both hydrophilic and hydrophobic drugs. They also have the potential of targeting the drug at a specific site, thus possessing a number of advantages for the potentially safe and effective drug delivery [17].

1.2.2 Dendrimers

Dendrimers are nano-sized, radially symmetric molecules with well-defined, homogeneous, and monodisperse structure [20]. Their main structure consists of a core molecule and alternating layer of monomer repeat units which are known as "Generations" and are characterized as G1, G2, G3, etc. Dendrimers have attracted a lot of attention in the past few years due to their low polydispersity, water solubility, and high surface functionalities which are advantageous for drug delivery [21].

1.2.3 Polymer micelles

Polymer micelles are formed via the self-assembly of amphiphilic block copolymers in an aqueous environment. They have a nanoscopic, usually spherical, core/shell structure in which the hydrophobic core acts as a microreservoir for the encapsulation of hydrophobic drugs and bioactive molecules, and the hydrophilic shell interfaces with the aqueous medium [22]. Some of the features that have rendered polymer micelles useful as drug delivery systems are the versatility of the core/shell structure, their stability in water-based media as well as their size which ranges from 20-200 nm which is crucial for biological applications.

1.2.4 Polymer nanoparticles

Polymer nanoparticles are solid and spherical (in most cases) structures prepared from natural or synthetic polymers. Drug delivery is known to be one of the most important biomedical applications of polymer nanoparticles. They have been tested to deliver a wide range of drugs, such as small hydrophilic and hydrophobic drugs, vaccines, peptides, and biological macromolecules, via several routes of administration. Different grades of poly(lactide-*co*-glycolide) and poly(lactide) copolymers are the most successfully used biodegradable polymers to prepare polymer nanoparticle-based drug delivery systems [23].

1.3 Polymer hydrogels

Hydrogels are water-swollen 3D networks of polymer chains that are either covalently or physically crosslinked. Hydrogels are excellent soft materials with diverse applications in various fields due to their tunable chemical structure and physical properties as well as their excellent biocompatibility [24].

Hydrogel synthesis is an essential step in developing new structures with beneficial properties. The hydrogel structure is defined by the hydration of hydrophilic groups and domains of the polymers involved. Therefore, these groups and their interconnected chains create three-dimensional networks via crosslinking, preventing their dissolution in the aqueous phase [25,26]. The standard synthesis procedures employ polymerization and crosslinking. These processes can happen in parallel in one step, or one after the other in multiple steps [25]. The polymerization process is part of the gelation process. The structure and the conformation of the starting material influence the formation of water swellable polymer networks. The monomers and polyfunctional comonomers act as crosslinkers in the network development. Sometimes polymerization is generated by radical initiators [27] or photoinitiators [28]. Hydrophilic polymers are often used for hydrogel synthesis due to their biocompatibility [29] in aqueous environments and mostly due to their drug loading potential [16]. The crosslinking agent plays a significant role in hydrogel swelling [30] and degradation [31]. It influences the physical properties of the final hydrogel product. Crosslinking methods employ covalent or non-covalent interactions between monomers providing elastic characteristics to the final polymer network [25,26,32].

For this reason, two different types of hydrogels are identified: chemical gels based on covalent interactions and physical gels based on non-covalent interactions [26].

One of the most significant features of hydrogels is their ability to absorb water that is often hundreds of times heavier than their weight. (**Fig. 1.3**) To measure the absorption, the swelling degree (SD) of the hydrogel is being used, which is the ratio of the gel's swollen mass to the polymer network dry mass [33]:

$$Swelling\ Degree\ (SD) = \frac{m_{swollen}}{m_{dry}}$$

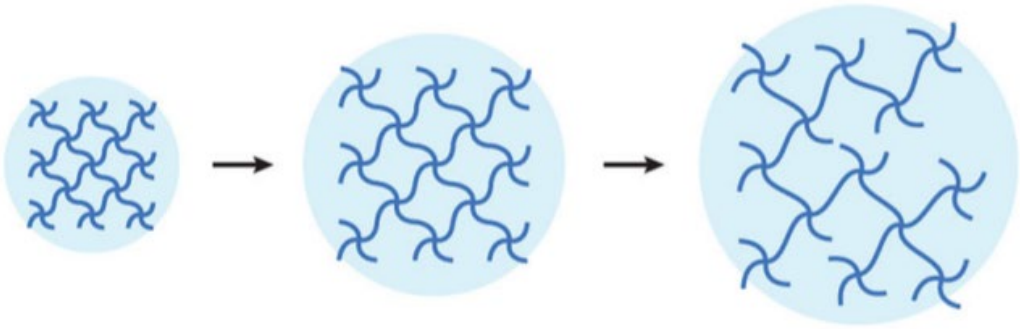

Figure 1.3: Changes in the shape of the hydrogel during swelling [34].

Due to their remarkable characteristics, including tunable physical, chemical, and biological properties, high biocompatibility, versatility in fabrication, and similarity to the native extracellular matrix (ECM), hydrogels have emerged as promising materials in the biomedical field. Hydrogels are used for a wide range of biomedical applications (**Fig. 1.4**), such as three-dimensional (3D) matrices for tissue engineering, composite biomaterials, biosensors, implants, and as injectable fillers in minimally invasive surgeries. The rational design of hydrogels with controlled physical and biological properties can be used to modulate cellular functionality and tissue morphogenesis [35]. Types of hydrogels with a wide range of biomedical applications are the self-healing hydrogels, multi-responsive and mechanically strong hydrogels and controlled-adhesive hydrogels for wound healing.

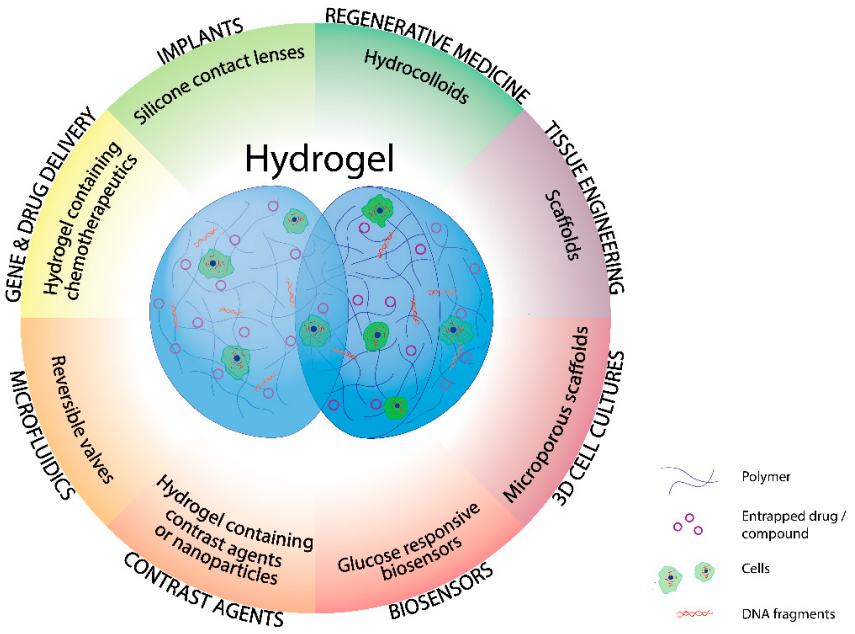

Figure 1.4: Biomedical applications of hydrogels [36].

The unique physical properties of hydrogels are very applicable in drug delivery systems too. Their highly porous structure can easily be tuned by controlling the density of the crosslinks in the gel matrix and the affinity of the hydrogels with the aqueous environment in which they are swollen. Their porosity also permits the loading of drugs into the gel matrix and subsequent drug release at a rate dependent on the diffusion coefficient of the small molecule or macromolecule through the gel network. Their biocompatibility is promoted by their high water content and the physiochemical similarity of hydrogels to the native extracellular matrix, both compositionally and mechanically. Biodegradability or dissolution may be designed in the hydrogels via enzymatic, hydrolytic, or environmental (e.g. pH, temperature, or light) pathways. Hydrogels are relatively deformable and can conform to the shape of the surface onto which they are applied [37].

Response to a stimulus is a basic process of living systems. Based on the lessons from Mother Nature, scientists have been designing useful materials that respond to external stimuli such as temperature, pH, light, electric field, etc. These responses are

manifested as dramatic changes in one of the following: shape, surface characteristics, solubility, formation of an intricate molecular self-assembly or a sol-to-gel transition [38]. Stimuli-degradable hydrogels is a class of stimuli-responsive hydrogels that have attracted considerable attention as intelligent materials in the biochemical and biomedical fields, since they can sense an environmental change and induce permanent or reversible lysis of their 3D structure [39].

1.3.1 Photodegradable hydrogels

Light is an external, non-invasive stimulus that can trigger the degradation of a material precisely, providing spatial and temporal control. When photodegradable hydrogels are exposed to irradiation, light-triggered reactions induce the dissociation of the polymer chains and therefore, the degradation of the polymer network in the exposed region. This results in either its complete degradation or in a local decrease of the crosslinking density, which influences the physical properties of the gel [35].

During the last decade, photodegradable hydrogels have attracted incredible attention and have emerged as useful platforms for research on tissue engineering, cell delivery and others. In 2020, Yavitt et al., presented an allyl sulfide photodegradable hydrogel which achieved rapid degradation through radical addition-fragmentation chain transfer reactions, to support routine passaging of intestinal organoids [40]. In 2017, Ji et al., designed a PEG-based hydrogel combined with caging chemistry, which could achieve light-triggered local control of the hydrogel for external manipulation of cellular microenvironments with real-time monitoring [41]. To this date, the majority of photodegradable hydrogels is based on synthetic polymers, such as poly(ethylene glycol) (PEG) [42].

1.3.2 PEG-based hydrogels

In the last decades, hydrogels have emerged as versatile biomaterials in various biomedical fields. Such cell compatible hydrogels have been prepared using a variety of polymeric materials, which can broadly be divided into two categories according to their origin: natural materials, such as hyaluronic acid [43,44] and chitosan [45], or synthetic materials, such as poly(ethylene glycol) (PEG) and poly(vinyl alcohol)

(PVA) [46]. The naturally derived hydrogels show excellent biocompatibility and biodegradability. However, they possess limited tunability of their degradation kinetics, relatively poor mechanical properties, batch-to-batch variations from different manufacturers, and potential immunogenic reactions which restrict their applications [47,48]. On the other hand, synthetic polymers are commercially available and can afford tunable mechanical properties and greater flexibility in the working range of pH, ionic strength, and chemical conditions, which makes them excellent candidates for hydrogel preparation. Among the synthetic polymers used for hydrogel preparation, PEG is the most popular one. PEG (**Fig. 1.5**) can be easily functionalized via its hydroxyl end-groups to yield numerous homofunctional or heterofunctional terminal groups, including thiols [49], vinylsulfones [50], maleimides [51], acrylates [52], allyls [53], and norbornenes [54]. Since PEG lacks any protein binding site, due to its hydrophilic and uncharged structure, it forms highly hydrated layers that restrict protein adsorption [27]. The excellent biocompatibility and low toxicity of PEG-based hydrogels render them ideal candidates for various biomedical applications [41].

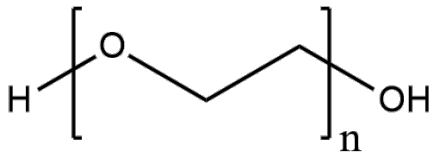

Figure 1.5: Chemical structure of poly(ethylene glycol).

1.4 Thioacetals

Thiols are the sulfur analogs of alcohols. The sulfur atom of a thiol is a better nucleophile than the oxygen atom of an alcohol. Thus, thiols react with aldehydes or ketones to form thioacetals or thioketals [55]. There are two thioacetal classes: monothioacetals and dithioacetals. Monothioacetals are less common and have the functional group RC(OR')(SR")H (**Fig. 1.6(a)**), while dithioacetals have the formula $RC(SR')_2H$ (symmetric dithioacetals) (**Fig. 1.6(b)**) or RC(SR')(SR")H (asymmetric dithioacetals) (**Fig. 1.6(c)**) [56]. The general reaction mechanism for the formation of the thioacetal bond is shown in **Fig. 1.6(d)** [57].

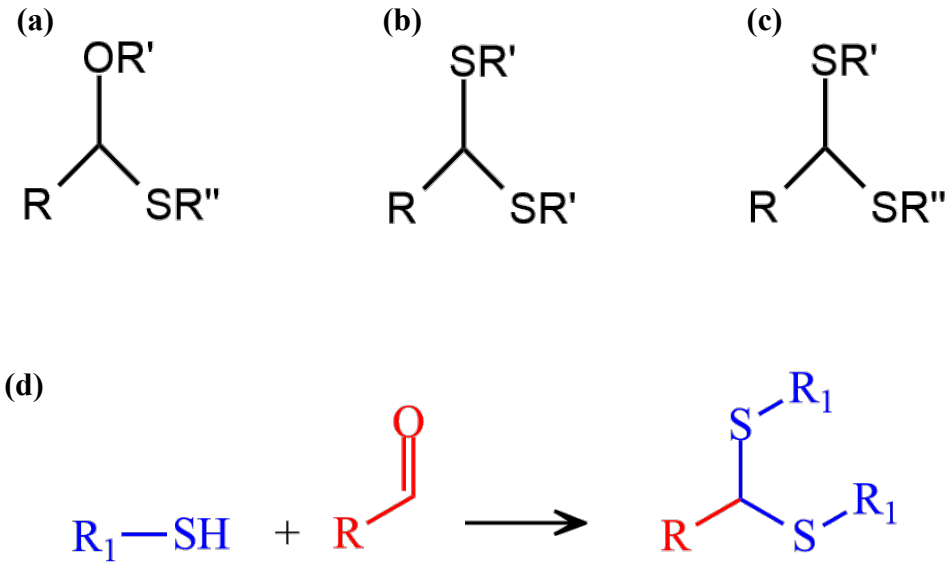

Figure 1.6: Chemical structure of (a) monothioacetals, (b) symmetric dithioacetals and (c) asymmetric dithioacetals. (d) The general reaction for the thioacetal bond formation.

The thioacetal and thioketal bonds are stable under acidic or basic conditions, but undergo bond cleavage in the presence of reactive oxygen species (ROS). Based on this, several studies have focused on the development of ROS-degradable thioacetal or thioketal polymeric materials. In 2010, Wilson et al., reported the synthesis of main-chain ROS-degradable polythioketals, which were used for the preparation of thioketal nanoparticles that could localize orally delivered siRNAs to sites of intestinal inflammation, and thus inhibit gene expression in inflamed intestinal tissue [58]. A few years later, Chen et al., synthesized a novel ROS-responsive poly(*β*-amino ester) by the introduction of a thioketal group in its monomer structure and used it as a carrier material to prepare nanoparticles for the co-loading and controlled release of the chemotherapeutic drug doxorubicin [59]. Recently, Men et al, presented photocleavable thioacetal block copolymers capable of forming nanoparticles in aqueous solution and releasing model drugs after UV irradiation. Unlike other thioacetal and thioketal polymers, these polymers were stable to reactive oxygen species (ROS), preventing the non-triggered release [60]. To date, to the best of our knowledge, photodegradable thioacetal-based hydrogels have not been reported yet.

1.5 Aim of this work

pH- and photo-cleavable materials based on thioacetal bonds have been reported for applications in the biomedical field. However, thioacetal-based hydrogels have not been synthesized yet. The aim of this thesis was the development of photodegradable thioacetal-based hydrogels, which are unpresented in the literature. For this purpose, dithiol end-functionalized PEGs were synthesized and used as hydrophilic macromonomers, which were cross-linked using an aromatic dialdehyde to afford thioacetal-based polymer networks. A series of hydrogels were prepared, which differed in their cross-link density, by varying the length of the PEG chains, and were characterized in terms of their porosity and degrees of swelling. The photodegradation profile of the water swollen hydrogels, upon UV light irradiation, was studied and was found to depend on the cross-link density of the hydrogels. Moreover, the ability of the hydrogels to encapsulate and release (with and without UV irradiation) hydrophilic and hydrophobic model dye molecules was investigated. These photodegradable thioacetal-based hydrogels are promising candidates for a range of applications, such as drug delivery, tissue engineering and wound healing.

Chapter 2: Experimental

2.1 Materials

Poly(ethylene glycol) of 1000, 1500 and 4000 gr/mol molecular weight were purchased from Sigma-Aldrich and were freeze-dried before use. Poly(ethylene glycol) dithiol functionalized with molecular weight of 1000 gr/mol, 3-mercaptopropionic acid (≥99.9%), terephthaldehyde and sulfamic acid (≥99.9%) as the catalyst were obtained from Sigma-Aldrich. Sulfuric acid (≥96%) was purchased from PENTA. 1,4-dithio-DL-threitol (≥96%) was obtained from Alfa Aesar. Sudan Red 7b, purchased from Sigma-Aldrich, and Orange II, purchased from Acros Organics were used as model drugs. Dichloromethane (≥99.9%), toluene (≥99.7%) and diethyl ether (≥99.8%) were purchased from Honeywell. Tetrahydrofuran and isopropanol were obtained from Carlo Erba Reagents and deuterated chloroform (≥99.8%) was purchased from Armar Chemicals. Milli-Q water with a resistivity of 18.2 MΩ.cm at 298 K was obtained from a Millipore apparatus and was used for all experiments.

2.2 Characterization methods

2.2.1 Proton Nuclear Magnetic Resonance (^{1}H NMR) spectroscopy

^{1}H NMR spectra were recorded on an Avance Bruker 500 MHz spectrometer. $CDCl_3$ was used as the solvent.

2.2.2 Scanning Electron Microscopy (SEM)

SEM images were obtained from a JEOL JSM-6390LV microscope at an accelerating voltage of 20 kV. The samples were sputter-coated with Au (thickness: 10 mm) before imaging.

2.2.3 Ultraviolet-Visible (UV-Vis) spectroscopy

The UV-Vis absorption spectra were recorded on a Shimadzu UV-2600 spectrophotometer in the wavelength range 200-700 nm. All samples were measured using quartz cuvettes.

2.3 Synthesis of dithiol end-functionalized PEG_{4k}

The synthesis of the dithiol end-functionalized PEG_{4k} was achieved through a Fisher esterification reaction of PEG_{4k} with 3-mercaptopropionic acid. Briefly, 1 gr (0.25 mmol) of freeze dried PEG_{4k} was dissolved in 20 ml of freshly distilled toluene, following the addition of 871 μL (10 mmol) 3-mercaptopropionic acid and 1-2 drops of H_2SO_4. The reaction solution was heated to 110 ºC under reflux conditions for 24 h. Afterwards, the reaction was concentrated under reduced pressure in the rotary evaporator and the modified $PEG_{4k}(SH)_2$ was precipitated 3 times in diethyl ether and washed with isopropanol. The resulted product was dried under vacuum overnight before ^1H NMR characterization and was stored under a N_2 atmosphere at -20 ºC until use. The oxidized samples (disulfide formation) were reduced using 1,4-dithiothreitol (DTT) in water at pH 8.5 for 5 h, at room temperature. Then water was removed from the solution under vacuum in the rotary evaporator. The final product was dissolved in dichloromethane, was precipitated in diethyl ether and was washed with isopropanol. The product was dried under vacuum before characterization by ^1H NMR and was stored under a N_2 atmosphere at -20 ºC until use. A similar experimental procedure was followed for the modification of PEG_{1k} and $PEG_{1.5k}$ by adjusting appropriately the PEG/3-mercaptopropionic acid mole ratio. **Table 2.1** shows the reaction conditions for the modification of each PEG and **Table 2.2** shows the conditions for the reduction process.

Table 2.1: Reaction conditions for the thiol end-functionalization of PEG

PEG M.W. (gr/mol)	PEG (mmol)	3-mercaptopropionic acid (mmol)	Toluene (ml)
1000	1	40	20
1500	0.67	26.8	20
4000	0.25	10	20

Table 2.2: Reaction conditions for the reduction of $PEG_n(SH)_2$

PEG M.W. (gr/mol)	$PEG_n(SH)_2$ (mmol)	1,4-dithiothreitol (mmol)	Water (ml)
1000	0.9	4.5	5
1500	0.6	3	5
4000	0.2	1	5

2.4 Synthesis of $PEG_n(SH)_2$ – terephthaldehyde ($PEG_n(SH)_2$-TPA) hydrogels

The thioacetal-based hydrogels were prepared by the condensation of the modified macromonomer PEG dithiol ($PEG_n(SH)_2$) with terephthaldehyde (TPA) under acidic condition using sulfamic acid as the acid catalyst. Briefly, the macromonomer $PEG_n(SH)_2$ was dissolved in a minimum amount of THF and the second comonomer TPA was added at a 1:1 or 2:1 mol ratio. The solution was vortexed until the complete dissolution of the monomers and then the acid catalyst was added. The solution was heated at 50 °C for 30 min to 1 h (depending on the molecular weight of the PEG dithiol) and the gelation time was recorded using the inverted vial method (**Fig. 2.1**). $PEG_n(SH)_2$-TPA hydrogels were fabricated using PEG_{4k}, $PEG_{1.5k}$ and PEG_{1k}. The $PEG_n(SH)_2$-TPA hydrogels were washed 20 times with THF and 20 times with water to remove the unreacted monomers and were then freeze dried before characterization. Moreover, a commercial PEG dithiol with molecular weight 1000 gr/mol (dithiol-PEG_{1k}), which does not contain the ester groups (**Fig. 2.2**), was used in some experiments. The reaction conditions for each hydrogel prepared are listed in **Table 2.3**.

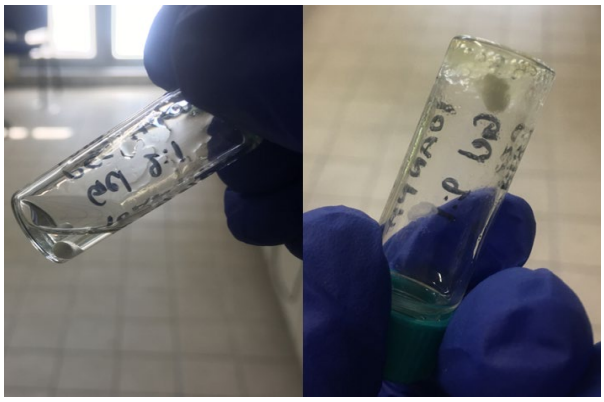

Figure 2.1: Characteristic photos of the synthesis of the $PEG_n(SH)_2$-TPA hydrogels: (a) before and (b) after gelation.

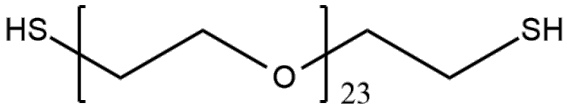

Figure 2.2: Chemical structure of dithiol-PEG_{1k} without the ester groups.

Table 2.3: Reaction conditions for the preparation of the $PEG_n(SH)_2$ –TPA hydrogels

M.W. (gr/mol)	$PEG_n(SH)_2$ (mmol)	Terephthaldehyde (mmol)
1000	0.09	0.045
1000*	0.1	0.05
1500	0.06	0.03
4000	0.02	0.01

*Commercially available dithiol PEG lacking the ester groups.

2.5 Swelling studies

In order to investigate their swelling degrees, 15 mgr of freeze dried $PEG_n(SH)_2$-TPA hydrogel were added in a vial with 5 ml of milliQ water. At predetermined time intervals, the mass of the swollen hydrogel was measured. The same procedure was followed for all the prepared hydrogels with the different molecular weight PEGs. The swelling degree of the hydrogel was calculated using the following equation:

$$Swelling\ Degree\ (SD) = \frac{m_{swollen}}{m_{dry}}$$

2.6 Photodegradation studies

10 mgr of the freeze dried $PEG_n(SH)_2$-TPA hydrogel were added in 5 ml of water and were allowed to swell for 50 min. The swollen hydrogel was placed in a quartz cuvette containing 3 ml water and was irradiated with a UV lamp at 254 nm at room temperature. At predetermined time intervals, the mass of the hydrogel was measured. The degradation (%) of the hydrogel was calculated using the following equation:

$$Degradation\ (\%) = \frac{m_0 - m_t}{m_0} \times 100\%$$

Where m_0 is the initial mass of the hydrogel and m_t is the mass of the hydrogel measured at each time point.

A similar procedure was followed to determine the degradation profile of all the hydrogels prepared in this study using PEG of different molecular weights.

2.7 Encapsulation of hydrophilic or hydrophobic dyes within the hydrogels

2.7.1 In situ $PEG_n(SH)_2$-TPA hydrogel formation with the hydrophobic dye Sudan Red 7b

A stock solution of Sudan Red 7b (SR) with concentration 2 mgr/ml was prepared in THF. The encapsulation of the dye was achieved in situ. Briefly, the same procedure as that described above for the hydrogel preparation was followed, but instead of pure THF, a predetermined amount of the stock solution of the dye in THF was used. The SR-loaded $PEG_n(SH)_2$-TPA hydrogels (**Fig. 2.3**) were washed 10 times with THF and 10 times with water to remove the unreacted monomers and non-loaded dye and then were freeze dried before characterization.

Figure 2.3: Photo of a SR-loaded $PEG_n(SH)_2$-TPA hydrogel.

The drug loading of the hydrogels was also calculated using the following equation:

$$Drug\ loading\ (\%) = \frac{m_{enc}}{m_{total}} \times 100\%$$

Where m_{enc} is the mass of the encapsulated dye, calculated as the total dye released from the hydrogels, and m_{total} is the mass of dye used during the preparation of the hydrogels.

2.7.2 Hydrophilic dye Orange II loading within the $PEG_n(SH)_2$-TPA hydrogels

A stock solution of Orange II (ORG) with concentration 5 mgr/ml was prepared in water. The encapsulation of the dye was achieved by adding 10 mg of the dried hydrogel into 5 ml of the dye solution for 50 min which caused the diffusion of the dye within the hydrogel. The ORG-loaded $PEG_n(SH)_2$-TPA hydrogels (**Fig. 2.4**) were freeze dried before characterization.

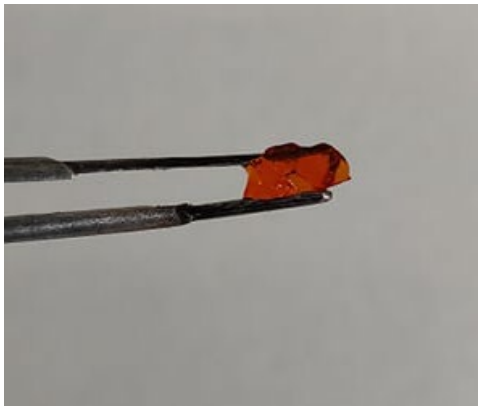

Figure 2.4: Photo of an ORG-loaded $PEG_n(SH)_2$-TPA hydrogel.

The drug loading of the hydrogels was again calculated using the equation presented in section 2.7.1.

2.8 Release studies from the dye loaded hydrogels

2.8.1 Release of Sudan Red 7b from the hydrogels

The release profile of the hydrophobic dye, Sudan Red 7b (SR), from the $PEG_n(SH)_2$-TPA hydrogels was studied. A sample of SR-loaded hydrogel (10 mgr) was placed in 5 ml of water and was allowed to swell for 50 min. The swollen hydrogel was transferred into a quartz cuvette with 3 ml of water and was irradiated with a UV lamp at 254 nm. At predetermined time intervals, the water in the cuvette was collected and was replaced with fresh water medium. The collected samples were dried under vacuum, dissolved in THF and analyzed by UV-Vis spectroscopy. The amount of the released dye was determined using a standard calibration curve of SR in THF and was calculated using the following equation:

$$Dye\ Release\ (\%) = \frac{C_t}{C_{total}} \times 100\%$$

Where C_t is the concentration of the released dye at each time point and C_{total} is the final concentration of the release dye.

In parallel, the release profile of SR from the hydrogels was studied in the absence of UV light irradiation, as a control sample. For this, the SR-loaded hydrogel was placed in water at 37 ºC and samples were collected at the predetermined time points and were analyzed by UV-Vis spectroscopy as described above for the UV irradiated sample.

2.8.2 Release of Orange II from the hydrogels

The release profile of the hydrophilic dye, Orange II (ORG), was also investigated. A sample of ORG-loaded dried $PEG_n(SH)_2$-TPA hydrogel (10 mgr) was placed in 5 ml of water and was allowed to swell for 50 min. The swollen hydrogel was transferred into a quartz cuvette containing 3 ml of water and was irradiated with a UV lamp at 254 nm. At predetermined time intervals, the water in the cuvette was collected and was replaced with fresh water. The collected samples were dried under vacuum, dissolved in THF and analyzed by UV-Vis spectroscopy. The amount of released dye was determined using a standard calibration curve of ORG in water and was calculated using the equation given in section 2.8.1 above.

The release profile of ORG from the hydrogels was also studied in the absence of UV light irradiation. For this, a sample of ORG-loaded hydrogel was placed in water at 37 ^{o}C and samples were collected at the predetermined time points and were analyzed by UV-Vis spectroscopy as described above for the UV irradiated sample.

Chapter 3: Results and discussion

3.1 Synthesis of the dithiol end-functionalized PEG

Three poly(ethylene glycol) (PEG) macromonomers, PEG_{1k}, $PEG_{1.5k}$ and PEG_{4k}, were functionalized by Fisher esterification with 3-mercaptopropionic acid to afford thiol end-groups. In a typical Fisher esterification, a carboxylic acid group (of 3-mercaptopropionic acid) reacts with an alcohol moiety (PEG) under acidic conditions (H_2SO_4). **Fig. 3.1** shows the schematic representation of the esterification process for the synthesis of the dithiol PEG ($PEG_n(SH)_2$) polymers.

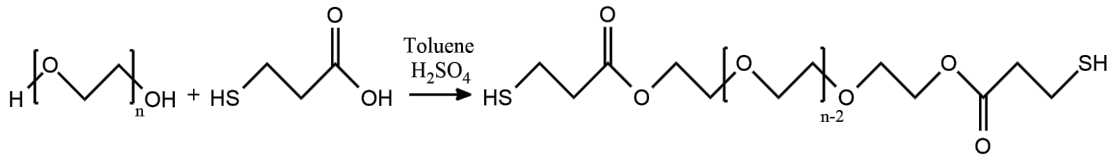

Figure 3.1: Synthesis of dithiol end-functionalized PEG.

The chemical structure and the composition of the $PEG_{1k}(SH)_2$, $PEG_{1.5k}(SH)_2$ and $PEG_{4k}(SH)_2$ polymers were determined by ^1H NMR spectroscopy. **Fig. 3.2(a)** shows the ^1H NMR spectrum of $PEG_{1k}(SH)_2$, **Fig. 3.2(b)** shows the ^1H NMR spectrum of $PEG_{1.5k}(SH)_2$ and **Fig. 3.2(c)** shows the ^1H NMR spectrum of $PEG_{4k}(SH)_2$. The peak at 1.68 ppm (a) is assigned to the two characteristic protons of the –SH end-groups, the peak at 2.69 ppm (b) corresponds to the four protons next to the thiol end-groups, the peak at 2.78 ppm (c) is assigned to the four protons next to the carbonyl groups, the peak at 4.27 ppm (d) corresponds to the four protons next to the ester groups and the peak at 3.65 ppm (e) is assigned to the protons of the PEG repeat units.

Table 3.1 shows the reaction yield and the degree of modification for each $PEG_n(SH)_2$ synthesized.

Table 3.1: Reaction yield and degree of modification for the $PEG_n(SH)_2$ polymers

PEG M.W. (gr/mol)	Reaction yield (%)	Degree of modification (%)
1000	70.8	85
1500	82.3	90
4000	72.3	100

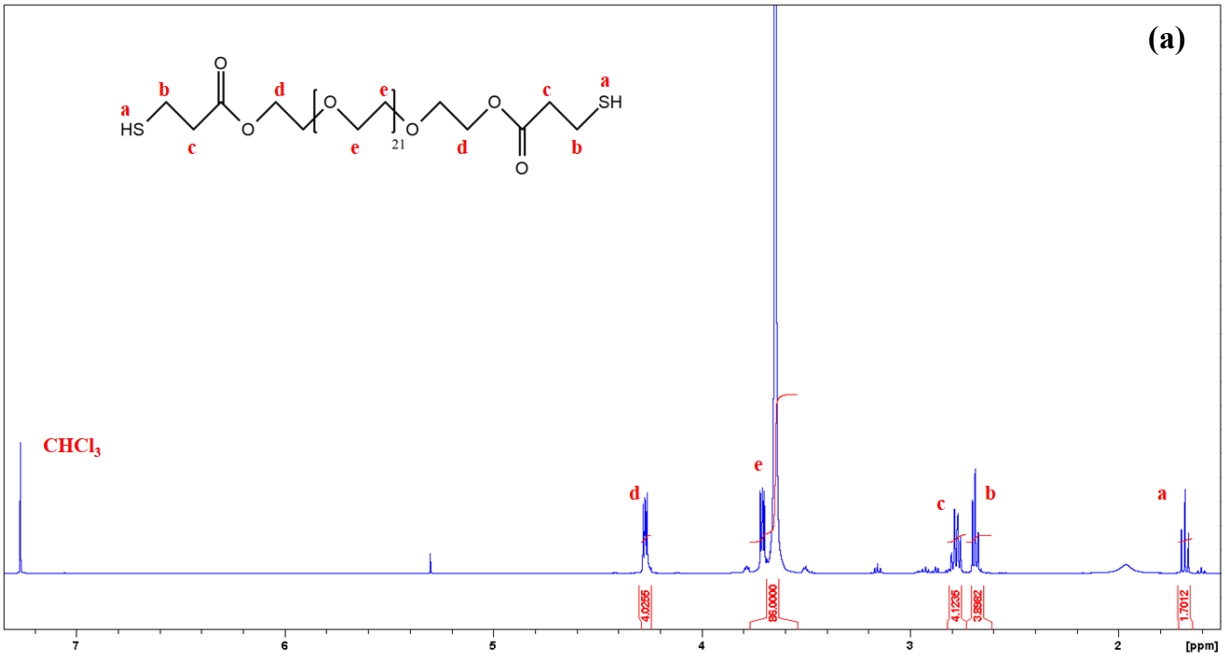

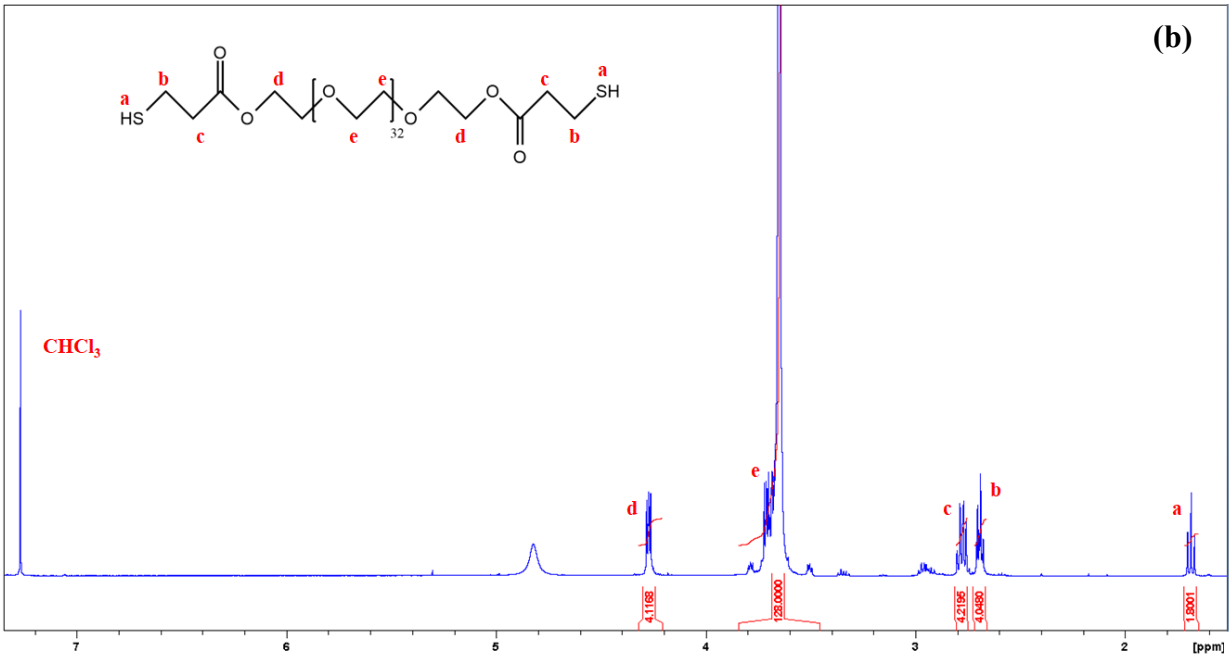

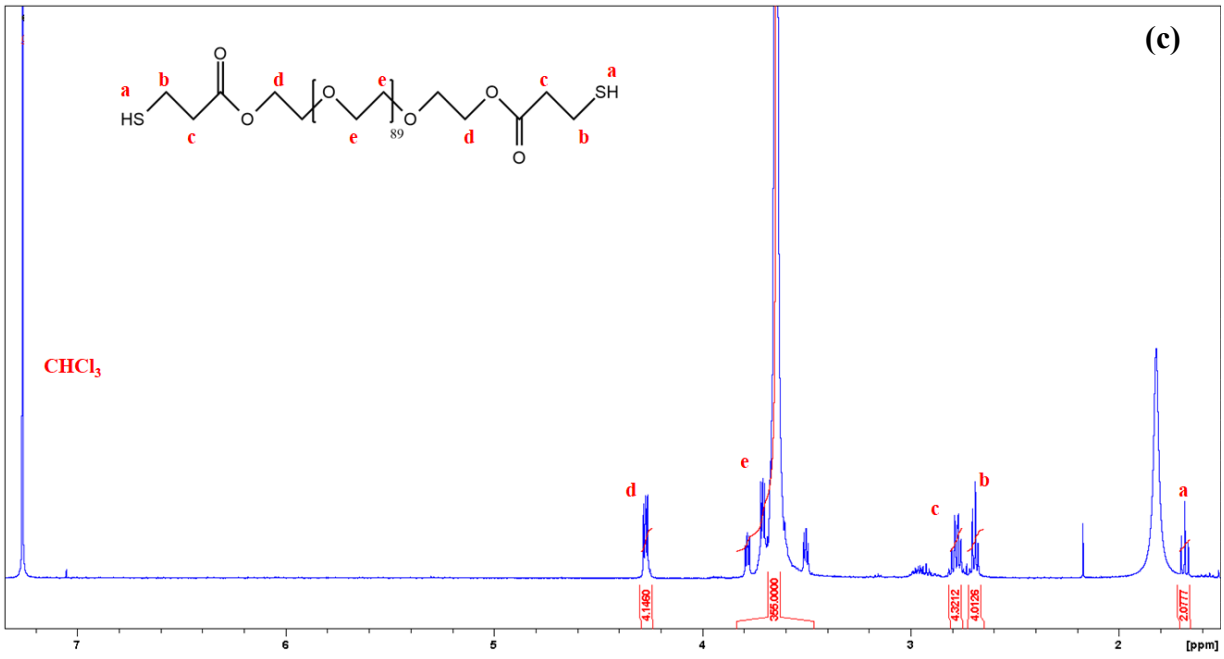

Figure 3.2: ^{1}H NMR spectra of (a) $PEG_{1k}(SH)_2$, (b) $PEG_{1.5k}(SH)_2$ and (c) $PEG_{4k}(SH)_2$ in $CDCl_3$.

3.2 Preparation of $PEG_n(SH)_2$ – terephthaldehyde ($PEG_n(SH)_2$-TPA) hydrogels

$PEG_n(SH)_2$-TPA hydrogels were prepared by the reaction of a $PEG_n(SH)_2$ macromonomer with a TPA monomer at a mol ratio 1:1 or 2:1. Each thiol end-group of $PEG_n(SH)_2$ reacts rapidly with two aldehyde groups of TPA to form cross-links comprising thioacetal bonds. **Fig. 3.3** shows the $PEG_n(SH)_2$-TPA hydrogel formation using sulfamic acid (S.A.) as a catalyst.

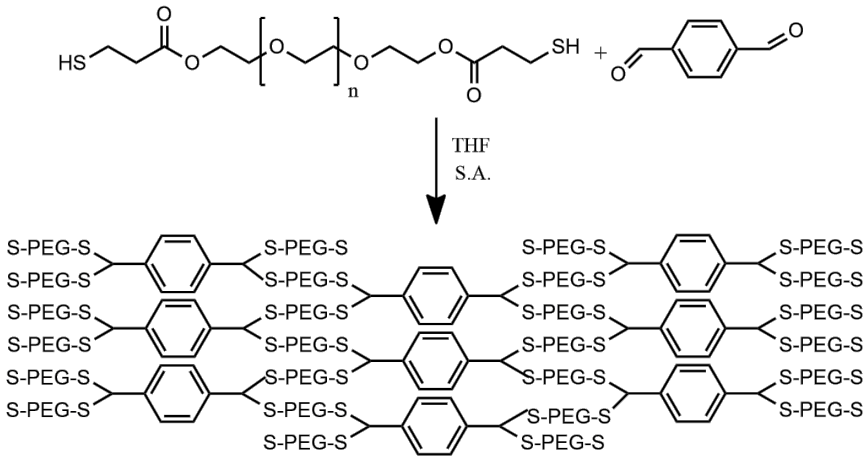

Figure 3.3: Schematic representation of the synthetic process followed to prepare the $PEG_n(SH)_2$-TPA hydrogels.

The gel formation at different temperatures, with and without the catalyst, was studied. We observed that at temperatures between 45 ºC and 55 ºC, the hydrogels were formed in 30 min to 1 h (depending on the molecular weight of the dithiol PEG). At temperatures above 60 ºC, the hydrogels were formed in 5 to 10 min. When preparing the hydrogels without the catalyst, it was found that the gel formation was deaccelerated and the $PEG_n(SH)_2$-TPA hydrogels were formed after 24 h at 55 ºC. **Table 3.2** shows some of the reaction conditions studied in this work for the preparation of the $PEG_{4k}(SH)_2$-TPA hydrogels.

Table 3.2: Reaction conditions employed for the preparation of the $PEG_{4k}(SH)_2$-TPA hydrogels

Mole ratio (TPA: $PEG_{4k}(SH)_2$)	Catalyst	Temperature (ºC)	Hydrogel formation time
1:1	Yes	50	1 h and 30 min
2:1	Yes	50	30 min
2:1	Yes	70	5 min
2:1	No	50	24 h

In order to study the effect of the molecular weight of PEG on the hydrogel formation and properties, we have prepared hydrogels using a $PEG_{1k}(SH)_2$, a $PEG_{1.5k}(SH)_2$, a $PEG_{4k}(SH)_2$ and a dithiol-PEG_{1k} which does not contain the ester groups. **Table 3.3** shows the reaction conditions used in this work for the preparation of the hydrogels using these lower molecular weight macromonomers.

Table 3.3: Reaction conditions employed for the preparation of the $PEG_n(SH)_2$-TPA hydrogels

PEG M.W. (gr/mol)	Mole ratio (TPA: $PEG_n(SH)_2$)	Catalyst	Temperature (ºC)	Hydrogel formation time
1500	2:1	Yes	50	50 min
1500	2:1	No	50	24 h
1000	2:1	Yes	50	40 min
1000*	2:1	Yes	50	1 h

*Commercially available dithiol PEG lacking the ester groups.

3.3 $PEG_n(SH)_2$-TPA hydrogel characterization

SEM characterization was used to investigate the morphology of the $PEG_n(SH)_2$-TPA hydrogels as well to correlate the PEG chain length with the pore size of the hydrogels. As shown in **Fig. 3.4**, the (dithiol-PEG_{1k})-TPA hydrogel did not exhibit a porous structure, whereas the $PEG_{1k}(SH)_2$-TPA hydrogel exhibited some porosity with a mean pore size ~ 3.8 μm (**Fig. 3.5(a)**). This difference in the porous structure of the hydrogels was attributed to the lack of the ester groups at the polymer chain of the dithiol-PEG_{1k}, which reduces the polymer chain length and results in a more rigid morphology. Moreover, TPA is an aromatic, hydrophobic molecule which also tends to aggregate due to π-π stacking and hydrophobic interactions in the aqueous medium thus prohibiting the effective open structure of the hydrogel. It is noted that this effect is more pronounced for the shorter chain length PEG macromonomer.

The $PEG_{1.5k}(SH)_2$-TPA and $PEG_{4k}(SH)_2$-TPA hydrogels appeared to be more porous with open and interconnected pores as shown at **Fig. 3.5(b)** and **Fig. 3.5(c)**. The mean pore size of the $PEG_{1.5k}(SH)_2$-TPA hydrogel was ~ 10.4 μm, while the mean pore size of the $PEG_{4k}(SH)_2$-TPA hydrogel was found ~ 15.5 μm. From the SEM images and the pore size distribution, we observed that by increasing the molecular weight of the PEG macromonomer, the porosity and pore size of the hydrogel increases. This is the result of increasing the polymer chain length which effectively decreases the cross-link density of the hydrogels. PEG-based hydrogels with similar porous structures to the $PEG_{4k}(SH)_2$-TPA hydrogel prepared in this work have been used for drug [61] and gene delivery [62], cell culture [63] and tissue engineering applications [64].

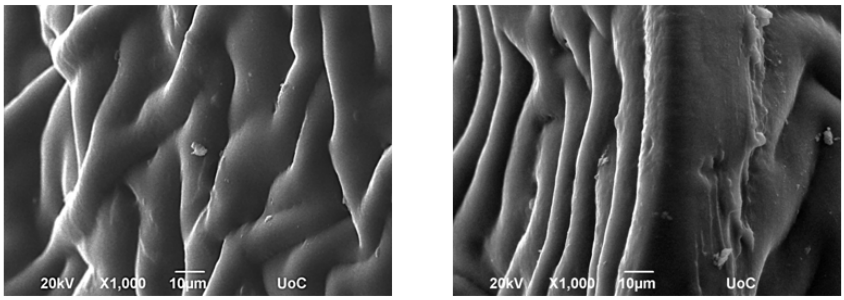

Figure 3.4: SEM images of (dithiol-PEG_{1k})-TPA hydrogel.

(a)

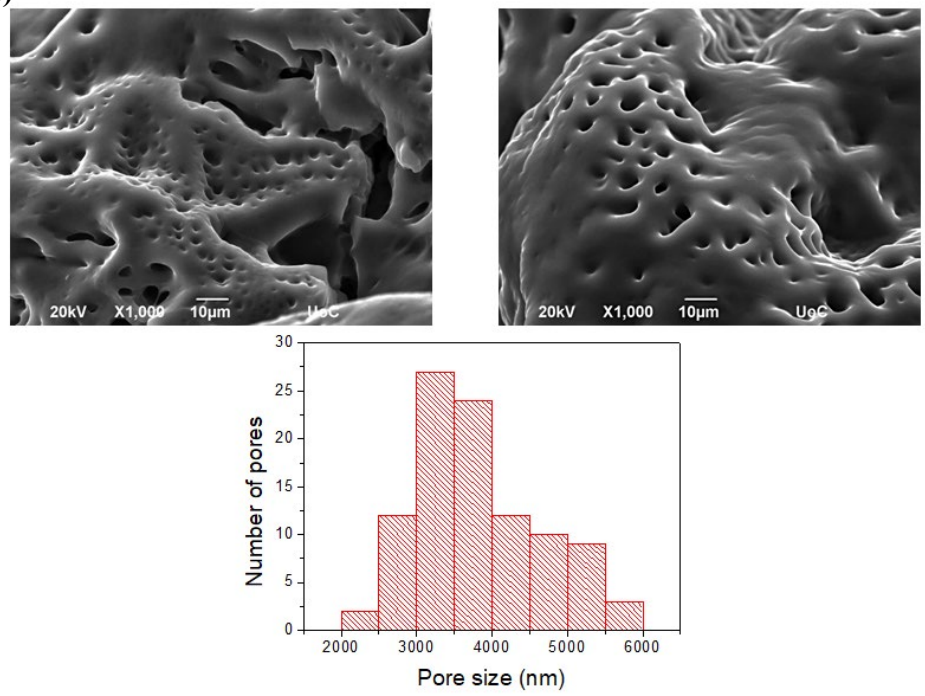
20kV X1,000 10μm UoC
20kV X1,000 10μm UoC
Number of pores
Pore size (nm)
0
5
10
15
20
25
30
2000
3000
4000
5000
6000

(b)

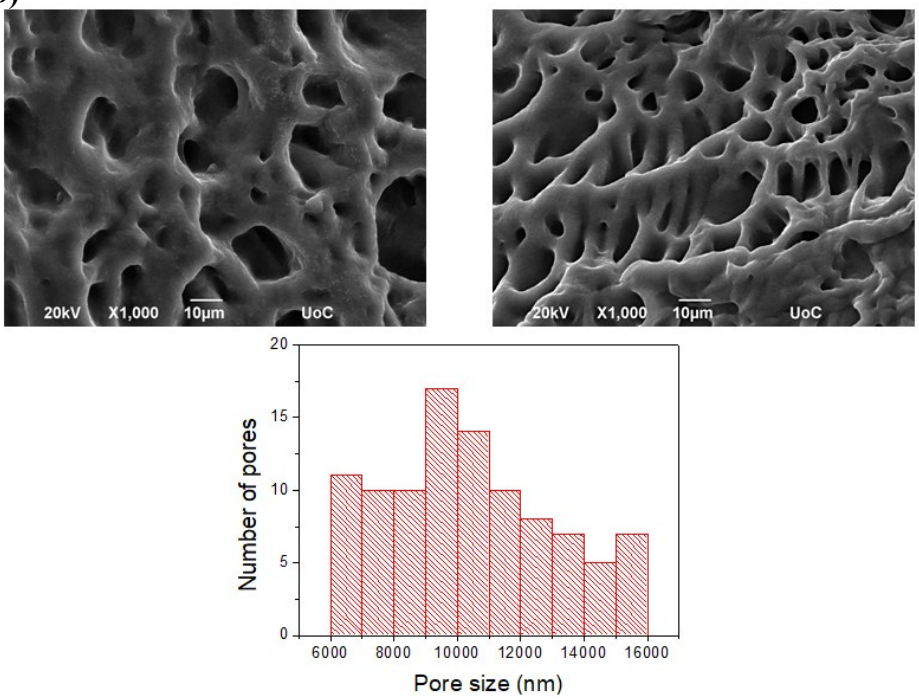
20kV X1,000 10μm UoC
20kV X1,000 10μm UoC
Number of pores
Pore size (nm)
0
5
10
15
20
6000
8000
10000
12000
14000
16000

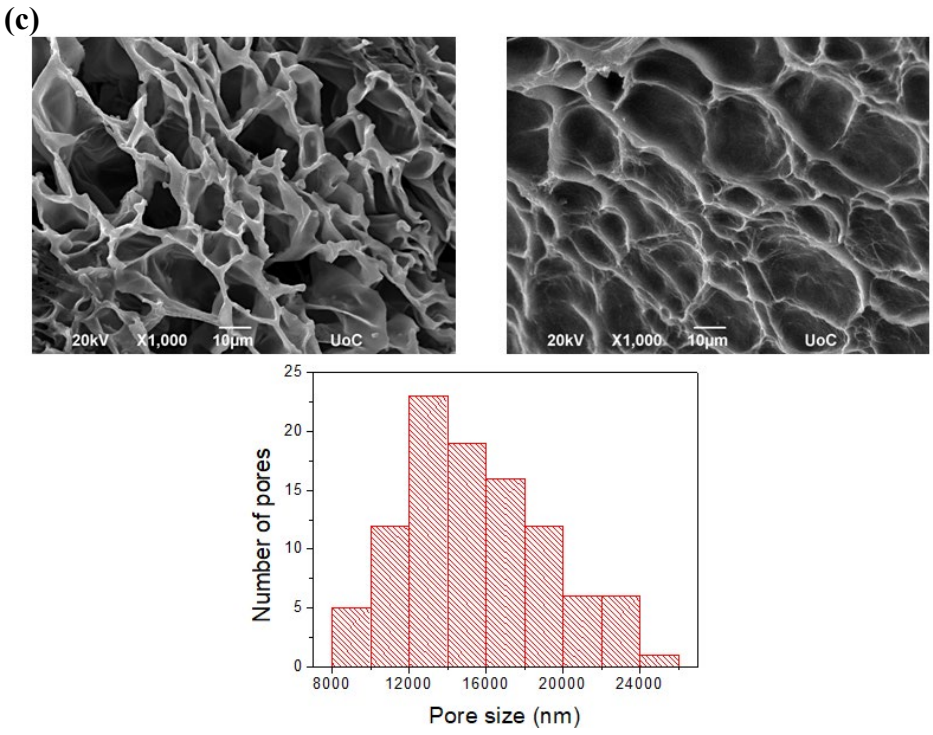

Figure 3.5: SEM images and pore size distribution of the synthesized (a) $PEG_{1k}(SH)_2$-TPA, (b) $PEG_{1.5k}(SH)_2$-TPA, (c) $PEG_{4k}(SH)_2$-TPA hydrogels.

3.4 Swelling studies

The swelling behavior of the $PEG_n(SH)_2$-TPA hydrogels for the different molecular weights of PEG macromonomer is shown in **Fig. 3.6**. As observed in the figure, when the molecular weight of the PEG macromonomer increases from 1000 gr/mol to 4000 gr/mol the swelling degree of the hydrogel increases as expected, due to the decrease in the effective cross-link density of the hydrogels. **Fig. 3.7** shows characteristic photos of the hydrogels after swelling. These degrees of swelling are consistent with the open pore structure and pore size of the hydrogels discussed above.

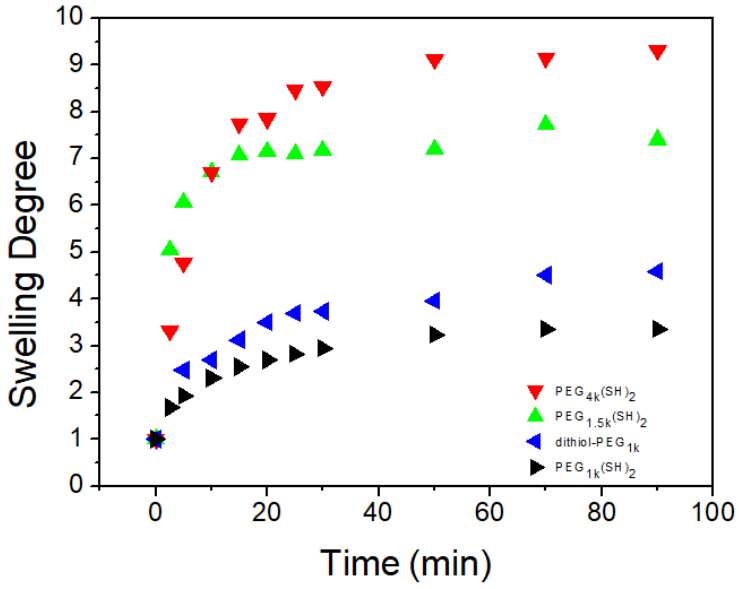

Figure 3.6: Swelling degrees of the $PEG_n(SH)_2$-TPA hydrogels as a function of time.

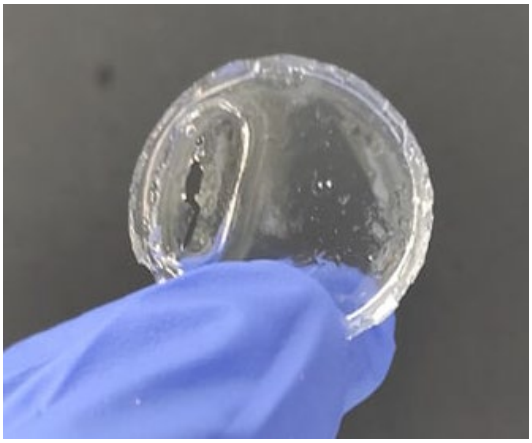

Figure 3.7: Characteristic photo of the $PEG_{4k}(SH)_2$-TPA hydrogel after swelling.

3.5 Photodegradation studies of the $PEG_n(SH)_2$–TPA hydrogels

The degradation behavior of the $PEG_n(SH)_2$–TPA hydrogels under UV irradiation for the different molecular weights of the PEG macromomomer was studied and the results are shown in **Fig. 3.8**. As observed in the figure, polymer degradation rate increased with the molecular weight of PEG macromonomer, indicating that the more hydrophilic and highly swellable hydrogels are easier to degrade. This is also verified below in the SR dye release experiments and establishes the photodegradable

character of these hydrogels, which should be studied in more detail in the future to accurately correlate the degradation behavior to the hydrogel structure.

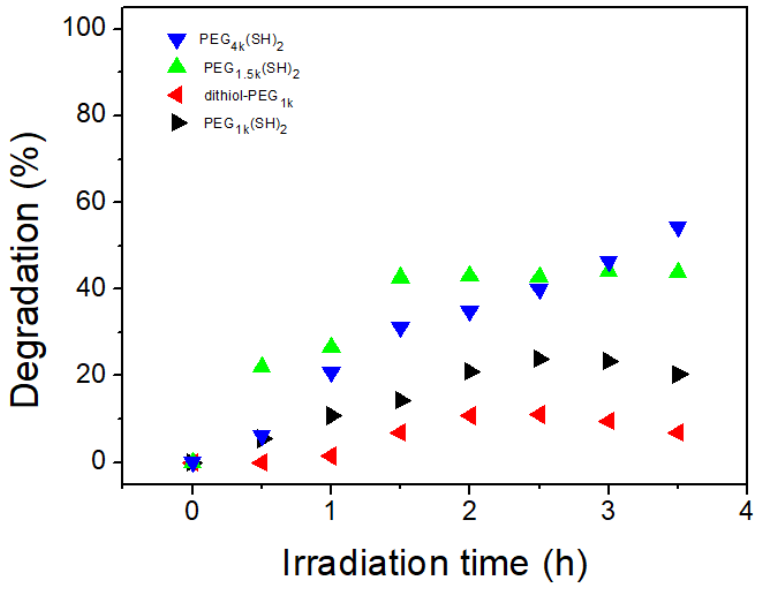

Figure 3.8: Degradation profile the of $PEG_n(SH)_2$-TPA hydrogels prepared in this work as a function of UV irradiation time.

3.6 Dye release studies

The main objective of this study was the development of thioacetal-based photodegradable hydrogels capable to encapsulate either hydrophobic or hydrophilic molecules, such as anticancer drugs, vitamins and other therapeutic compounds and release them upon light stimulation. In order to study the photoinduced release of hydrophobic and hydrophilic molecules from the hydrogels, two different dyes, Sudan Red 7b (SR), as a hydrophobic dye, and Orange II (ORG), as a hydrophilic dye, were loaded within the prepared hydrogels. The encapsulation of the SR and ORG dyes was achieved as described in the experimental section.

3.6.1 Release of the hydrophobic dye loaded in the $PEG_n(SH)_2$-TPA hydrogels

In order to investigate the photo-triggered release of the hydrophobic dye from the thioacetal-based hydrogels, SR was loaded within the hydrophobic domains of the network. The release study was conducted for the $PEG_{1k}(SH)_2$-TPA and the $PEG_{4k}(SH)_2$-TPA hydrogels. In each case, the hydrogels were placed into cuvettes with neutral water as the medium and were exposed to UV light irradiation (254 nm). It is noted that the SR dye absorbs at 254 nm, however, its absorption is not high enough to prevent the degradation of the hydrogel and the release of the dye. At the same time, another hydrogel sample was placed in a vessel with water medium and was used as the control, without light irradiation. At predetermined time points, the water medium from the irradiated sample and the control sample (taking care to also recover the precipitated dye at the bottom of the cuvette) was collected and replaced with fresh water. The collected samples were lyophilized, dissolved in THF and were analyzed by UV-Vis spectroscopy. **Fig. 3.9** shows typical UV-Vis spectra of the released SR dye from the $PEG_{4k}(SH)_2$-TPA hydrogel.

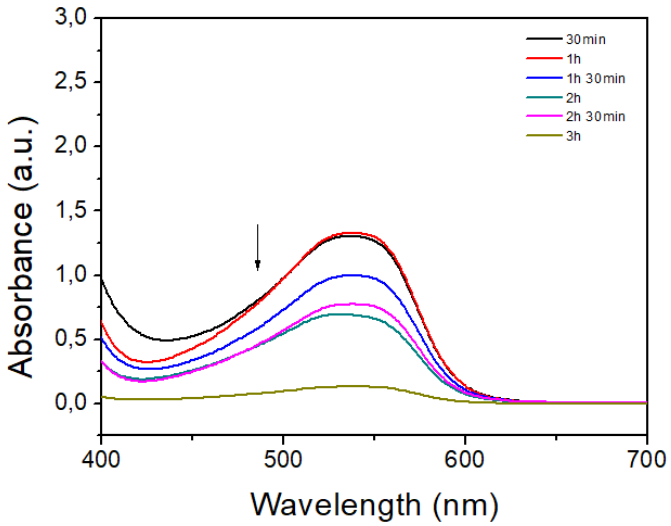

Figure 3.9: Typical UV-Vis spectra of the released SR dye from the irradiated $PEG_{4k}(SH)_2$-TPA hydrogel.

The drug loading and release profiles of the $PEG_n(SH)_2$-TPA hydrogels were calculated based on the standard calibration curve of SR in THF. **Fig. 3.10** shows the spectra at known dye concentration in THF and the calibration curve of SR.

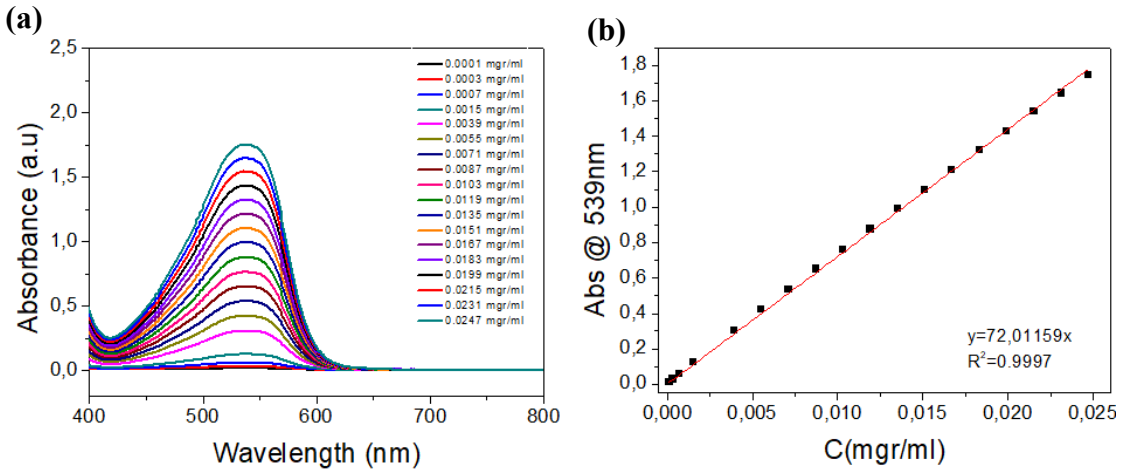

Figure 3.10: (a) UV-Vis absorption spectra of SR in THF at various concentrations and (b) standard calibration curve of SR in THF.

The drug loadings of the hydrogels were calculated using the equation presented in section 2.7.1 and are shown in **Table 3.4**. The results are in agreement with the literature considering that other studied PEG-based hydrogels have been found to exhibit a drug loading in the range between 2% and 20% [65,66].

Table 3.4: SR drug loading of the hydrogels

Hydrogel	Drug loading (%)
$PEG_{1k}(SH)_2$-TPA	9.9
$PEG_{4k}(SH)_2$-TPA	36.3

Quantitatively, the absorbance maximum of the released dye from the hydrogels at 539 nm was followed and was found to decrease over with the irradiation time, indicating the release of the dye from the hydrogel and the precipitation of the released dye in the aqueous medium. By solubilizing the released dye in THF, and measuring its absorbance by UV-Vis spectroscopy, the release profile of the dye was calculated using the calibration curve shown in **Fig. 3.10(b)**. **Fig. 3.11(a)** shows the release profile of SR, with and without irradiation, from the $PEG_{1k}(SH)_2$-TPA hydrogels. As observed, the release of the SR dye from the hydrogel, with or without irradiation, is dramatically low. In particular, both the non-irradiated $PEG_{1k}(SH)_2$-TPA hydrogel and the irradiated $PEG_{1k}(SH)_2$-TPA hydrogel released less than 1% of

the loaded dye after 14 h. Moreover, it was visually observed, that the mass and the color of the dye loaded hydrogel samples remained the same after the UV irradiation process. This result indicates that the $PEG_{1k}(SH)_2$-TPA hydrogels do not release the dye effectively upon UV irradiation. On the other hand, **Fig. 3.11(b)** shows the release profile of SR, with and without UV irradiation, from the $PEG_{4k}(SH)_2$-TPA hydrogels. As shown in the figure, after 3 h UV irradiation, the loaded SR dye was completely released from the $PEG_{4k}(SH)_2$-TPA hydrogel, accompanied by the complete hydrogel degradation (**Fig. 3.11(b) inset**). In contrast, the non-irradiated $PEG_{4k}(SH)_2$-TPA hydrogel released only ~ 2% of the loaded dye after 48 h, indicating that the $PEG_{4k}(SH)_2$-TPA hydrogel can be successfully loaded with hydrophobic molecules and release them remotely upon UV light irradiation. Controlling the release of a hydrophobic molecule, such as drug molecules, from a hydrogel with the use of a spatiotemporally controlled external stimulus, such as light irradiation, opens new, important perspectives for their further clinical applications.

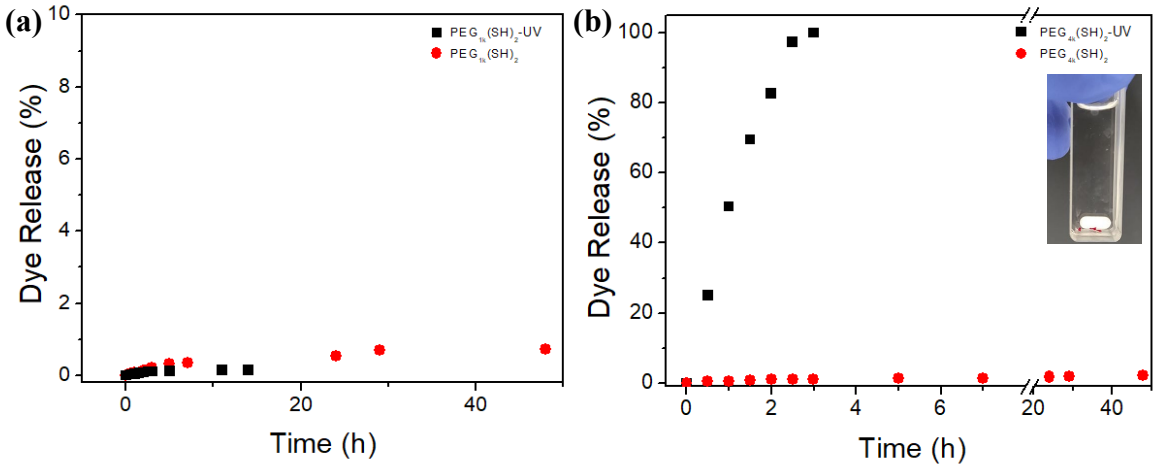

Figure 3.11: Release profile of SR, with and without UV irradiation, from the (a) $PEG_{1k}(SH)_2$-TPA and (b) $PEG_{4k}(SH)_2$-TPA hydrogels. The inset in (b) shows the irradiated $PEG_{4k}(SH)_2$-TPA hydrogel after 3h.

.

Overall, we have found that the $PEG_{4k}(SH)_2$-TPA hydrogel exhibited a faster release kinetics of the hydrophobic dye upon UV irradiation, compared to the $PEG_{1k}(SH)_2$-TPA hydrogel. This result is in good agreement with the photodegradation behavior of the hydrogels discussed above in section 3.5, and can be correlated with the porosity and the pore size of each hydrogel. The $PEG_{1k}(SH)_2$-TPA hydrogel showed a

lower porosity and smaller pore size, indicating a more compact structure. This has hindered the effective degradation of the hydrogel and the release of the dye, in contrast to the $PEG_{4k}(SH)_2$-TPA hydrogel. However, future studies are required to quantify the porosity of the two hydrogels by porosimetry measurements, and to establish a more solid relationship between the structure of the hydrogel sample and its degradation and release behavior.

3.6.2 Release of the hydrophilic dye loaded in the $PEG_n(SH)_2$-TPA hydrogels

The photo-triggered release of a hydrophilic dye from the thioacetal-based hydrogels was studied by loading the hydrophilic dye ORG in the hydrogels. The release study was conducted for the $PEG_{1k}(SH)_2$-TPA and the $PEG_{4k}(SH)_2$-TPA hydrogels. In each case, the hydrogels were placed in cuvettes with neutral water as the medium and were exposed to UV light irradiation (254 nm). At the same time, other hydrogel samples were placed in vessels with water medium and were used as control samples in the absence of UV irradiation. At predetermined time points, the water medium from the irradiated sample and the control sample was collected and replaced with fresh water. The collected samples were lyophilized, dissolved in water and analyzed by UV–Vis spectroscopy. The drug loading and release profiles of the $PEG_n(SH)_2$-TPA hydrogels were calculated based on a standard calibration curve of ORG in water. **Fig. 3.12** shows the spectra at known dye concentration in water and the calibration curve of ORG.

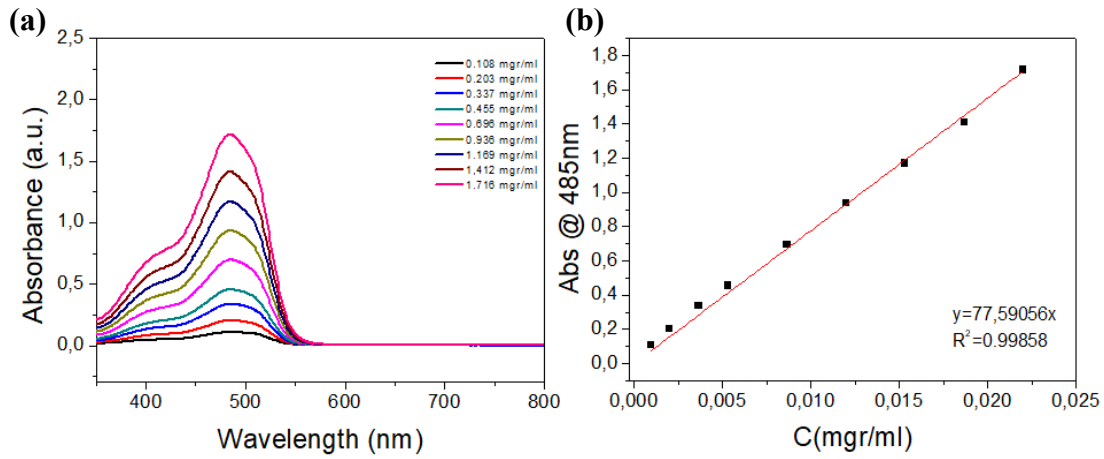

Figure 3.12: (a) UV-Vis absorption spectra of ORG in water at various concentrations and (b) standard calibration curve of ORG in water.

The drug loadings of the hydrogels were calculated using the equation presented in section 2.7.1 and are shown in **Table 3.5**. The results in agreement with the literature considering that other studied PEG-based hydrogels have been shown to exhibit drug loadings in the range between 2% and 20% [65,66].

Table 3.5: ORG drug loading of the hydrogels

Hydrogel	Drug loading (%)
$PEG_{1k}(SH)_2$-TPA	5.6
$PEG_{4k}(SH)_2$-TPA	10.1

The absorbance maximum of the released dye from the hydrogels at 485 nm was measured. As shown in **Fig. 3.13(a)**, the release kinetics of ORG, with and without UV light irradiation, from the $PEG_{1k}(SH)_2$-TPA hydrogels is similar, with only a slightly faster dye release for the UV irradiated sample (at 60 min 79% and 94% was released from the non-irradiated and irradiated sample, respectively). Thus, in the case of the hydrophilic ORG dye, the effect of light irradiation does not play a significant role on the release of the dye, as the release profile is dominated by the diffusion rate of the dye from the hydrogel, which is fast compared to the degradation rate of the hydrogel. Similar profiles were also found for the $PEG_{4k}(SH)_2$-TPA hydrogels (**Fig. 3.13(b)**) with the effect of UV irradiation having a small effect on the release kinetics (at 60 min 89% and 99% was released from the non-irradiated and irradiated sample, respectively) signifying again that the diffusion of the hydrophilic dye in the aqueous medium is of similar rate to the degradation rate of the hydrogel.

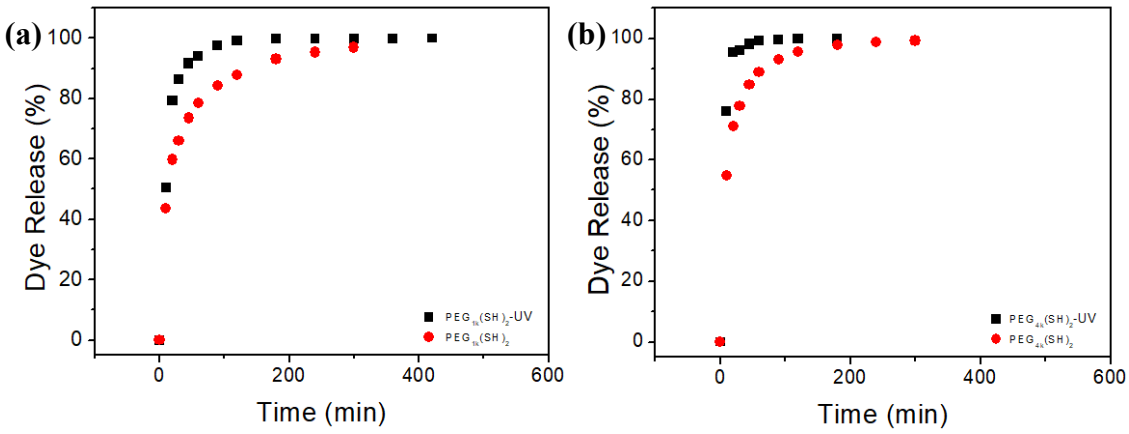

Figure 3.13: Release profile of ORG with and without UV irradiation from the (a) $PEG_{1k}(SH)_2$-TPA and (b) $PEG_{4k}(SH)_2$-TPA hydrogels.

So overall, the hydrophilic ORG dye loaded hydrogels were found to release the cargo faster than the SR-loaded hydrogel (for example, at 60 min irradiation 50% and 99% was released from the UV irradiated $PEG_{4k}(SH)_2$-TPA hydrogel loaded with SR and ORG, respectively), as the release kinetics of the hydrophilic dye were dominated by its diffusion from the hydrogel in the surrounding aqueous medium. To be able to control the release of a hydrophilic cargo, future studies could focus on the light-induced release of a hydrophilic molecule which is chemically bound onto the hydrogel via a photo-labile bond.

Chapter 4: Conclusions and future studies

Hydrogels are attractive biomaterials due to their tunable properties, inherent biocompatibility, and similarity with the soft tissues and cell environment. Over the past decades, hydrogels have developed from being static and inert materials towards new and "smart" responsive materials able to adapt to various stimuli, such as the solution pH and temperature, enzyme or light. Light stimulation is particularly interesting for many applications, because its allows the contact-free, remote manipulation of the biomaterials' properties, with inherent spatial and temporal control [24].

In this thesis, dithiol end-functionalized PEG ($PEG_n(SH)_2$) macromonomers of different molecular weights were synthesized and used for the preparation of thioacetal-based hydrogels. The modified PEG macomonomers were characterized by ^1H NMR spectroscopy. A small, difunctional aromatic comonomer, terephthaldehyde (TPA) was used as the crosslinker and different reaction conditions were investigated for the preparation of $PEG_n(SH)_2$-TPA hydrogels. The morphology of the synthesized hydrogels was studied by SEM and their mean pore sizes in the dry state were determined. The mean pore size was found to be smaller for the $PEG_{1k}(SH)_2$-TPA hydrogel (3.8 μm) and increased with the molecular weight of the PEG macromonomer to give $PEG_{1.5k}(SH)_2$-TPA hydrogels with a mean pore size of 10.4 μm, and $PEG_{4k}(SH)_2$-TPA hydrogels with a mean pore size of 15.5 μm.

The swelling behavior of the hydrogels in water was also studied. The $PEG_{4k}(SH)_2$-TPA hydrogel exhibited the higher degree of swelling, which decreased monotonically with the decrease of the molecular weight of the PEG macromonomer, due to the increase of the cross-link density of the hydrogels.

Next, the photodegradation behavior of the thioacetal-based hydrogels was investigated as a function of irradiation time. We found that the % photodegradation increased, for the same irradiation time, as the molecular weight of the PEG macromonomer of the hydrogels increased. This is in good agreement with the increase in the degree of swelling and the porosity and pore size of the hydrogels, signifying that the more swollen and higher porosity samples degrade faster, however,

the underlying mechanism that leads to this influence of the hydrogel structure on its photodegradation behavior is still unclear and needs further investigation.

Finally, the release profile of a hydrophobic (SR) and a hydrophilic (ORG) dye from the hydrogels was studied. For this, dye-loaded hydrogels were prepared and the release profile of the dye was monitored as a function of time at 37 °C, to simulate the body temperature, under UV irradiation at 254 nm. The results showed that the hydrophobic dye (SR) was released at 100% after 3 h irradiation from the $PEG_{4k}(SH)_2$-TPA hydrogel, whereas a release of approximately 2% was recorded after 48 h for the non-irradiated $PEG_{4k}(SH)_2$-TPA hydrogel. This indicated the control of the dye release by the light stimulus and agreed well with the photodegradation behavior of the hydrogel. In contrast, the irradiated and non-irradiated $PEG_{1k}(SH)_2$-TPA hydrogels exhibited a much slower release of the SR molecules (less than 1% after 14 h), signifying again that the photodegradation of the hydrogels controls the release of the hydrophobic cargo. On the other hand, for the hydrophilic dye (ORG) the results showed that the release kinetics of the cargo are faster compared to the hydrophobic dye, and similar with and without irradiation, from both the $PEG_{1k}(SH)_2$-TPA and $PEG_{4k}(SH)_2$-TPA hydrogels, with the light stimulus having only a small effect in the release rate of the dye. This suggests that in the case of the hydrophilic cargo the release is dominated by its diffusion from the hydrogels into the surrounding aqueous medium, which is fast enough compared to the photodegradation rate of the hydrogels.

The results of this work are very interesting and promising for the use of these photodegradable thioacetal-based hydrogels in drug delivery, cell encapsulation, wound healing and tissue engineering applications. Future work will explore the influence of the hydrogel structure on its photodegradation rate, the possibility to control the release of chemically bound hydrophilic molecules onto the hydrogels, as well as the mechanical properties of the hydrogels prepared and their *in vitro* and *in vivo* behavior upon light irradiation.

Chapter 5: Characterization techniques

5.1 Proton Nuclear Magnetic Resonance (^{1}H NMR) spectroscopy

Nuclear magnetic resonance (NMR) spectroscopy relies on a property of certain atomic nuclei that causes them to absorb and then re-release electromagnetic energy at characteristic frequencies. Shifts in the usual response frequency for a given isotope provide information about their immediate environment, including the influence from nearby electrons and magnetic nuclei, and make it possible to infer molecular identity, geometry, and more. ^{1}H NMR spectroscopy, also referred as proton NMR, is the most frequently used type of NMR, due to the abundance of hydrogen nuclei in organic compounds and its subsequent sensitivity.

The NMR technique allows observing local magnetic fields around atomic nuclei. The sample, typically a liquid or a solid dissolved in a solvent, is placed in a magnetic field and the NMR signal is generated by radiowave excitation of the nuclei of the sample into nuclear magnetic resonance, which is detected with sensitive radio receivers. The signal offers the necessary information about the nuclei's environment. The nucleus' exact field strength (in ppm) comes into resonance with a reference standard, which is usually the signal of the protonated fraction of the deuterated solvent employed. The nuclei are shielded from the external magnetic field by electron clouds, allowing them to absorb higher energy (lower ppm), whereas neighboring functional groups deshield the nuclei, allowing them to absorb lower energy (higher ppm). Nuclei that are chemically and magnetically equal resonant at the same energy and produce a single signal or pattern. Following the n+1 rule with coupling constant J, protons on nearby carbons interact and split each other's resonances into several peaks. Spin-spin coupling occurs frequently between nuclei that are one, two and three bonds apart. Since the area beneath an NMR peak is proportional to the number of nuclei that give rise to that resonance, the proton ratios that produce the resonance can be calculated by integration.

5.2 Scanning Electron Microscopy (SEM)

Scanning electron microscopy (SEM) is one of the most common methods used to image the microstructure of materials. SEM is an electron microscopy technique that images a sample's surface by scanning a focused energetic electron beam. SEM is one of the most popular tools to study surface morphology and to identify small areas that cannot be resolved by optical microscopy.

SEM works by scanning a sample with an electron beam. An electron gun fires this beam, which then accelerates down the column of the scanning electron microscope. During this action, the electron beams pass through a series of lenses and apertures, which focus it. This occurs under high vacuum conditions, which prevents and molecules or atoms already present in the microscope column from interacting with the electron beam, and ensures a high-quality imaging by protecting the electron source from vibrations and noise. The electron beam scans the sample in a raster pattern, scanning the surface area in lines from side to side, top to bottom. The electrons interact with the atoms on the surface of the sample. This interaction creates signals in the form of secondary electrons, backscattered electrons and rays that are characteristic of the sample. Detectors in the microscope pick up these signals and create high resolution images displayed on a computer screen.

5.3 Ultraviolet-Visible (UV-Vis) spectroscopy

Ultraviolet-Visible (UV-Vis) spectroscopy is a quantitative spectroscopic technique used to measure how much of a chemical substance absorbs light. This is done by measuring the intensity of light that passes through a sample with respect to the intensity of light through a reference sample or blank. UV-Vis spectroscopy encompasses absorption spectroscopy and reflectance spectroscopy in the UV-Vis spectral region (200 nm to 800 nm). Molecules containing π-electrons can absorb ultraviolet or visible light energy. These absorptions lead to electron transitions.

In general, UV-Vis spectroscopy is used to determine elemental concentrations quantitatively in a solution according to the Beer–Lambert law:

$$A = log_{10}\left(\frac{I_0}{I}\right) = \varepsilon \cdot c \cdot L$$

where A is the measured absorbance, I_0 is the intensity of the incident light at a given wavelength, I is the transmitted intensity, L is the path length through the sample, c is the concentration of the absorbing species, and ε is a constant known as the molar absorptivity or extinction coefficient for each species and wavelength [67].

References

[1] M. Wei, Y. Gao, X. Li, M.J. Serpe, Stimuli-responsive polymers and their applications, Polym. Chem. 8 (2017) 127–143. https://doi.org/10.1039/c6py01585a.

[2] P. Theato, Synthesis of Well-Defined Polymeric Activated Esters, J. Polym. Sci. Part A Polym. Chem. 46 (2008) 6677–6687. https://doi.org/10.1002/pola.22994.

[3] S. Dai, P. Ravi, K.C. Tam, pH-Responsive polymers: Synthesis, properties and applications, Soft Matter. 4 (2008) 435–449. https://doi.org/10.1039/b714741d.

[4] M. Heskins, J.E. Guillet, Solution Properties of Poly(N-isopropylacrylamide), J. Macromol. Sci. Part A - Chem. 2 (1968) 1441–1455. https://doi.org/http://dx.doi.org/10.1080/10601326808051910.

[5] Y.L. Colson, M.W. Grinstaff, Biologically responsive polymeric nanoparticles for drug delivery, Adv. Mater. 24 (2012) 3878–3886. https://doi.org/10.1002/adma.201200420.

[6] R.N. Oliveira, R. Rouzé, B. Quilty, G.G. Alves, G.D.A. Soares, R.M.S.M. Thiré, G.B. McGuinness, Mechanical properties and in vitro characterization of polyvinyl alcoholnano- silver hydrogel wound dressings, Interface Focus. 4 (2014). https://doi.org/10.1098/rsfs.2013.0049.

[7] J. Hu, S. Liu, Responsive polymers for detection and sensing applications: Current status and future developments, Macromolecules. 43 (2010) 8315–8330. https://doi.org/10.1021/ma1005815.

[8] M. Ma, L. Guo, D.G. Anderson, R. Langer, Bio-inspired polymer composite actuator and generator driven by water gradients, Science (80-.). 339 (2013) 186–189. https://doi.org/10.1126/science.1230262.

[9] Q. Zhao, J.W.C. Dunlop, X. Qiu, F. Huang, Z. Zhang, J. Heyda, J. Dzubiella, M. Antonietti, J. Yuan, An instant multi-responsive porous polymer actuator driven by solvent molecule sorption, Nat. Commun. 5 (2014) 1–8.

https://doi.org/10.1038/ncomms5293.

[10] Z. Hu, X. Zhang, Y. Li, Synthesis and application of modulated polymer gels, Science (80-.). 269 (1995) 525–527. https://doi.org/10.1126/science.269.5223.525.

[11] A.K. Bajpai, S.K. Shukla, S. Bhanu, S. Kankane, Responsive polymers in controlled drug delivery, Prog. Polym. Sci. 33 (2008) 1088–1118. https://doi.org/10.1016/j.progpolymsci.2008.07.005.

[12] D. Parasuraman, M.J. Serpe, Poly (N-isopropylacrylamide) microgels for organic dye removal from water, ACS Appl. Mater. Interfaces. 3 (2011) 2732–2737. https://doi.org/10.1021/am2005288.

[13] X. Sun, S. Agate, K.S. Salem, L. Lucia, L. Pal, Hydrogel-Based Sensor Networks: Compositions, Properties, and Applications - A Review, ACS Appl. Bio Mater. 4 (2021) 140–162. https://doi.org/10.1021/acsabm.0c01011.

[14] G. Tiwari, R. Tiwari, S. Bannerjee, L. Bhati, S. Pandey, P. Pandey, B. Sriwastawa, Drug delivery systems: An updated review, Int. J. Pharm. Investig. 2 (2012) 2. https://doi.org/10.4103/2230-973x.96920.

[15] T.M. Allen, P.R. Cullis, Drug Delivery Systems: Entering the Mainstream, Science (80-.). 303 (2004) 1818–1822. https://doi.org/10.1126/science.1095833.

[16] W.B. Liechty, D.R. Kryscio, B. V. Slaughter, N.A. Peppas, Polymers for drug delivery systems, Annu. Rev. Chem. Biomol. Eng. 1 (2010) 149–173. https://doi.org/10.1146/annurev-chembioeng-073009-100847.

[17] A.K. Goyal, G. Rath, C. Faujdar, B. Malik, Application and Perspective of pH-Responsive Nano Drug Delivery Systems, Elsevier Inc., 2019. https://doi.org/10.1016/b978-0-12-814029-1.00002-8.

[18] S.W. Kim, Y.H. Bae, T. Okano, Hydrogels: Swelling, Drug Loading, and Release, Pharm. Res. 9 (1992) 283–289.

[19] G. Bozzuto, A. Molinari, Liposomes as nanomedical devices, Int. J. Nanomedicine. 10 (2015) 975–999. https://doi.org/10.2147/IJN.S68861.

[20] E. Abbasi, S.F. Aval, A. Akbarzadeh, M. Milani, H.T. Nasrabadi, S.W. Joo, Y. Hanifehpour, K. Nejati-Koshki, R. Pashaei-Asl, Dendrimers: Synthesis, applications, and properties, Nanoscale Res. Lett. 9 (2014) 1–10. https://doi.org/10.1186/1556-276X-9-247.

[21] R. Esfand, D.A. Tomalia, Poly(amidoamine) (PAMAM) dendrimers: From biomimicry to drug delivery and biomedical applications, Drug Discov. Today. 6 (2001) 427–436. https://doi.org/10.1016/S1359-6446(01)01757-3.

[22] H.M. Aliabadi, A. Lavasanifar, Polymeric micelles for drug delivery, Expert Opin. Drug Deliv. 3 (2006) 139–162. https://doi.org/10.1517/17425247.3.1.139.

[23] L. Peltonen, M. Singhal, J. Hirvonen, Principles of nanosized drug delivery systems, Elsevier Ltd., 2020. https://doi.org/10.1016/b978-0-08-102985-5.00001-2.

[24] L. Li, J.M. Scheiger, P.A. Levkin, Design and Applications of Photoresponsive Hydrogels, Adv. Mater. 31 (2019). https://doi.org/10.1002/adma.201807333.

[25] E.M. Ahmed, Hydrogel: Preparation, characterization, and applications: A review, J. Adv. Res. 6 (2015) 105–121. https://doi.org/10.1016/j.jare.2013.07.006.

[26] W.E. Hennink, C.F. van Nostrum, Novel crosslinking methods to design hydrogels, Adv. Drug Dlivery Rev. 54 (2002) 13–36. https://doi.org/https://doi.org/10.1016/S0169-409X(01)00240-X.

[27] G.T. Jeong, K.M. Lee, H.S. Yang, S.H. Park, J.H. Park, C. Sunwoo, H.W. Ryu, D. Kim, W.T. Lee, H.S. Kim, W.S. Cha, D.H. Park, Synthesis of poly(sorbitan methacrylate) hydrogel by free-radical polymerization, Appl. Biochem. Biotechnol. 137–140 (2007) 935–946. https://doi.org/10.1007/s12010-007-9109-4.

[28] A.S. Sawhney, C.P. Pathak, J.A. Hubbell, Bioerodible Hydrogels Based on Photopolymerized Poly(ethylene glycol)-co-poly (α-hydroxy acid) Diacrylate Macromers, Macromolecules. 26 (1993) 581–587. https://doi.org/10.1021/ma00056a005.

[29] B.V.K.J. Schmidt, Hydrophilic polymers, Polymers (Basel). 11 (2019) 1–5. https://doi.org/10.3390/polym11040693.

[30] J. Zhang, A. Wang, Study on superabsorbent composites. IX: Synthesis, characterization and swelling behaviors of polyacrylamide/clay composites based on various clays, React. Funct. Polym. 67 (2007) 737–745. https://doi.org/10.1016/j.reactfunctpolym.2007.05.001.

[31] K.R. Kamath, K. Park, Biodegradable hydrogels in drug delivery, Adv. Drug Deliv. Rev. 11 (1993) 59–84. https://doi.org/10.1016/0169-409X(93)90027-2.

[32] M.L. Oyen, Mechanical characterisation of hydrogel materials, Int. Mater. Rev. 59 (2014) 44–59. https://doi.org/10.1179/1743280413Y.0000000022.

[33] M. Vamvakaki, S. Parouti, K. Crysopoulou, Laboratory exercises of soft matter synthesis and characterization, 2004.

[34] H. Kamata, X. Li, U. Il Chung, T. Sakai, Design of Hydrogels for Biomedical Applications, Adv. Healthc. Mater. 4 (2015) 2360–2374. https://doi.org/10.1002/adhm.201500076.

[35] N. Annabi, A. Tamayol, J.A. Uquillas, M. Akbari, L.E. Bertassoni, C. Cha, G. Camci-Unal, M.R. Dokmeci, N.A. Peppas, A. Khademhosseini, 25th anniversary article: Rational design and applications of hydrogels in regenerative medicine, Adv. Mater. 26 (2014) 85–124. https://doi.org/10.1002/adma.201303233.

[36] A. Onaciu, R.A. Munteanu, A.I. Moldovan, C.S. Moldovan, I. Berindan-Neagoe, Hydrogels based drug delivery synthesis, characterization and administration, Pharmaceutics. 11 (2019). https://doi.org/10.3390/pharmaceutics11090432.

[37] T.R. Hoare, D.S. Kohane, Hydrogels in drug delivery: Progress and challenges, Polymer (Guildf). 49 (2008) 1993–2007. https://doi.org/10.1016/j.polymer.2008.01.027.

[38] B. Jeong, A. Gutowska, Lessons from nature: Stimuli-responsive polymers and their biomedical applications, Trends Biotechnol. 20 (2002) 305–311.

https://doi.org/10.1016/S0167-7799(02)01962-5.

[39] T. Miyata, T. Uragami, K. Nakamae, Biomolecule-sensitive hydrogels, Adv. Drug Deliv. Rev. 54 (2002) 79–98. https://doi.org/10.1016/S0169-409X(01)00241-1.

[40] F.M. Yavitt, T.E. Brown, E.A. Hushka, M.E. Brown, N. Gjorevski, P.J. Dempsey, M.P. Lutolf, K.S. Anseth, The Effect of Thiol Structure on Allyl Sulfide Photodegradable Hydrogels and their Application as a Degradable Scaffold for Organoid Passaging, Adv. Mater. 32 (2020) 1–10. https://doi.org/10.1002/adma.201905366.

[41] H. Ji, K. Xi, Q. Zhang, X. Jia, Photodegradable hydrogels for external manipulation of cellular microenvironments with real-time monitoring, RSC Adv. 7 (2017) 24331–24337. https://doi.org/10.1039/c7ra02629c.

[42] D.S. Shin, J. You, A. Rahimian, T. Vu, C. Siltanen, A. Ehsanipour, G. Stybayeva, J. Sutcliffe, A. Revzin, Photodegradable hydrogels for capture, detection, and release of live cells, Angew. Chemie - Int. Ed. 53 (2014) 8221–8224. https://doi.org/10.1002/anie.201404323.

[43] F. Rehfeldt, A.E.X. Brown, M. Raab, S. Cai, A.L. Zajac, A. Zemel, D.E. Discher, Hyaluronic acid matrices show matrix stiffness in 2D and 3D dictates cytoskeletal order and myosin-II phosphorylation within stem cells, Integr. Biol. 4 (2012) 422–430. https://doi.org/10.1039/c2ib00150k.

[44] X. Xu, A.K. Jha, D.A. Harrington, M.C. Farach-Carson, X. Jia, Hyaluronic acid-based hydrogels: From a natural polysaccharide to complex networks, Soft Matter. 8 (2012) 3280–3294. https://doi.org/10.1039/c2sm06463d.

[45] Z. Shariatinia, A.M. Jalali, Chitosan-based hydrogels: Preparation, properties and applications, Int. J. Biol. Macromol. 115 (2018) 194–220. https://doi.org/10.1016/j.ijbiomac.2018.04.034.

[46] S. Saraf, A. Alexander, Ajazuddin, J. Khan, S. Saraf, Poly(ethylene glycol)-poly(lactic-co-glycolic acid) based thermosensitive injectable hydrogels for biomedical applications, J. Control. Release. 172 (2013) 715–729. https://doi.org/10.1016/j.jconrel.2013.10.006.

[47] R. Langer, D.A. Tirrell, Designing materials for biology and medicine, Nature. 428 (2004) 487–492. https://doi.org/10.1038/nature02388.

[48] Z. Shi, X. Gao, M.W. Ullah, S. Li, Q. Wang, G. Yang, Electroconductive natural polymer-based hydrogels, Biomaterials. 111 (2016) 40–54. https://doi.org/10.1016/j.biomaterials.2016.09.020.

[49] B.D. Fairbanks, S.P. Singh, C.N. Bowman, K.S. Anseth, Photodegradable, photoadaptable hydrogels via radical-mediated disulfide fragmentation reaction, Macromolecules. 44 (2011) 2444–2450. https://doi.org/10.1021/ma200202w.

[50] M.P. Lutolf, J.A. Hubbell, Synthesis and physicochemical characterization of end-linked poly(ethylene glycol)-co-peptide hydrogels formed by Michael-type addition, Biomacromolecules. 4 (2003) 713–722. https://doi.org/10.1021/bm025744e.

[51] K.M. Schultz, A.D. Baldwin, K.L. Kiick, E.M. Furst, Gelation of covalently cross-linked PEG-heparin hydrogels, Macromolecules. 42 (2009) 5310–5315. https://doi.org/10.1021/ma900766u.

[52] A. Metters, J. Hubbell, Network formation and degradation behavior of hydrogels formed by Michael-type addition reactions, Biomacromolecules. 6 (2005) 290–301. https://doi.org/10.1021/bm049607o.

[53] A.E. Rydholm, S.K. Reddy, K.S. Anseth, C.N. Bowman, Development and characterization of degradable thiol-allyl ether photopolymers, Polymer (Guildf). 48 (2007) 4589–4600. https://doi.org/10.1016/j.polymer.2007.05.063.

[54] S.B. Anderson, C.C. Lin, D. V. Kuntzler, K.S. Anseth, The performance of human mesenchymal stem cells encapsulated in cell-degradable polymer-peptide hydrogels, Biomaterials. 32 (2011) 3564–3574. https://doi.org/10.1016/j.biomaterials.2011.01.064.

[55] R.J. Ouellette, J.D. Rawn, Aldehydes and Ketones: Nucleophilic Addition Reactions, in: Org. Chem., 2014: pp. 629–657. https://doi.org/https://doi.org/10.1016/B978-0-12-800780-8.00019-X.

[56] G.P. Moss, P.A.S. Smith, D. Tavernier, Glossary of class names of organic compounds and reactive intermediates based on structure (IUPAC recommendations 1995), in: Pure Appl. Chem., 1995: p. 1371. https://doi.org/10.1351/pac199567081307.

[57] A. Leitemberger, L.M.C. Böhs, M.L.B. Peixoto, C.H. Rosa, G.R. Rosa, M. Godoi, Sulfamic Acid-Catalyzed Thioacetalization of Aldehydes under Solvent and Metal-Free Conditions, ChemistrySelect. 5 (2020) 8253–8257. https://doi.org/10.1002/slct.202001308.

[58] D.S. Wilson, G. Dalmasso, L. Wang, S. V. Sitaraman, D. Merlin, N. Murthy, Orally delivered thioketal nanoparticles loaded with TNF-α-siRNA target inflammation and inhibit gene expression in the intestines, Nat. Mater. 9 (2010) 923–928. https://doi.org/10.1038/nmat2859.

[59] B. Chen, Y. Zhang, R. Ran, B. Wang, F. Qin, T. Zhang, G. Wan, H. Chen, Y. Wang, Reactive oxygen species-responsive nanoparticles based on a thioketal-containing poly(β-amino ester) for combining photothermal/photodynamic therapy and chemotherapy, Polym. Chem. 10 (2019) 4746–4757. https://doi.org/10.1039/c9py00575g.

[60] Y. Men, T.G. Brevé, H. Liu, A.G. Denkova, R. Eelkema, Photo cleavable thioacetal block copolymers for controlled release, Polym. Chem. 12 (2021) 3612–3618. https://doi.org/10.1039/d1py00514f.

[61] J. Yu, X. Xu, F. Yao, Z. Luo, L. Jin, B. Xie, S. Shi, H. Ma, X. Li, H. Chen, In situ covalently cross-linked PEG hydrogel for ocular drug delivery applications, Int. J. Pharm. 470 (2014) 151–157. https://doi.org/10.1016/j.ijpharm.2014.04.053.

[62] Y. Li, C. Yang, M. Khan, S. Liu, J.L. Hedrick, Y.Y. Yang, P.L.R. Ee, Nanostructured PEG-based hydrogels with tunable physical properties for gene delivery to human mesenchymal stem cells, Biomaterials. 33 (2012) 6533–6541. https://doi.org/10.1016/j.biomaterials.2012.05.043.

[63] D.J. Menzies, A. Cameron, T. Munro, E. Wolvetang, L. Grøndahl, J.J. Cooper-White, Tailorable cell culture platforms from enzymatically cross-linked

multifunctional poly(ethylene glycol)-based hydrogels, Biomacromolecules. 14 (2013) 413–423. https://doi.org/10.1021/bm301652q.

[64] Y.C. Chiu, M.H. Cheng, H. Engel, S.W. Kao, J.C. Larson, S. Gupta, E.M. Brey, The role of pore size on vascularization and tissue remodeling in PEG hydrogels, Biomaterials. 32 (2011) 6045–6051. https://doi.org/10.1016/j.biomaterials.2011.04.066.

[65] M.P. Kai, A.W. Keeler, J.L. Perry, K.G. Reuter, J.C. Luft, S.K. O'Neal, W.C. Zamboni, J.M. Desimone, Evaluation of drug loading, pharmacokinetic behavior, and toxicity of a cisplatin-containing hydrogel nanoparticle, J. Control. Release. 204 (2015) 70–77. https://doi.org/10.1016/j.jconrel.2015.03.001.

[66] S. Salmaso, A. Semenzato, S. Bersani, P. Matricardi, F. Rossi, P. Caliceti, Cyclodextrin/PEG based hydrogels for multi-drug delivery, Int. J. Pharm. 345 (2007) 42–50. https://doi.org/10.1016/j.ijpharm.2007.05.035.

[67] H. Wang, P.K. Chu, Surface Characterization of Biomaterials, Elsevier, 2013. https://doi.org/10.1016/B978-0-12-415800-9.00004-8.